Empirical validation of co-simulation models for adaptive building envelopes

Borkowski, Esther; Luna-Navarro, Alessandra; Michael, Michalis; Overend, Mauro; Rovas, Dimitrios; Raslan, Rokia

DOI
10.47982/jfde.2022.1.06

Publication date
2022

Document Version
Final published version

Published in
Journal of Facade Design and Engineering

Citation (APA)
Borkowski, E., Luna-Navarro, A., Michael, M., Overend, M., Rovas, D., & Raslan, R. (2022). Empirical validation of co-simulation models for adaptive building envelopes. *Journal of Facade Design and Engineering*, *10*(1), 119-154. https://doi.org/10.47982/jfde.2022.1.06

Empirical validation of co-simulation models for adaptive building envelopes

Esther Borkowski [*1,2], Alessandra Luna-Navarro [3,4], Michalis Michael [3], Mauro Overend [4], Dimitrios Rovas [1], Rokia Raslan [1]

* Corresponding author, esther.borkowski.12@ucl.ac.uk
1 University College London, Institute for Environmental Design and Engineering, United Kingdom
2 ETH Zurich, Institute of Technology in Architecture, Architecture and Building Systems, Switzerland
3 University of Cambridge, Department of Engineering, Glass and Façade Technology Research Group, United Kingdom
4 Delft University of Technology, Faculty of Architecture and the Built Environment, The Netherlands

Abstract

The thermal performance of adaptive building envelopes can be evaluated using building performance simulation tools. Simulation capabilities and accuracy in predicting the dynamic behaviour of adaptive building envelopes can be enhanced through co-simulation. However, it is unclear how accurately co-simulation can predict the performance of adaptive building envelopes and how the accuracy of adaptive building envelope models created in co-simulation setups can be assessed and validated. Therefore, this study presents new evidence on the empirical validation of co-simulation setups for adaptive building envelopes by establishing an assessment framework to determine the extent to which they can accurately represent the real world. The framework was applied to a case study to validate a co-simulation setup for a blind automation system using monitored data from MATELab, a full-scale outdoor test facility with realistic indoor and outdoor conditions. The validation of the co-simulation model of MATELab resulted in a median CV-RMSE index, a measure of model accuracy, of 5.9%. This indicates that the simulated data points have a small variance relative to the measured data points, showing a good model fit. In the future, modellers from the façade community can use the assessment framework for their co-simulation setups.

Keywords

Adaptive building envelope, Empirical validation, Co-simulation, Outdoor test facility, In-situ characterisation.

DOI

http://doi.org/10.47982/jfde.2022.1.06

1 INTRODUCTION

Adaptive building envelopes can improve thermal building performance by dynamically adapting their behaviour over time to changing environmental conditions (Loonen, Favoino, Hensen, & Overend, 2017). For example, adaptive building envelopes may significantly reduce energy demand for lighting, heating and cooling by conveniently modulating the incoming solar radiation (Favoino, Fiorito, Cannavale, Ranzi, & Overend, 2016).

Despite the rapid development of novel adaptive building envelope technologies, they are hardly adopted in practice. One reason is that capital costs for adaptive building envelopes are typically higher than for static building envelopes due to additional components – involving more raw materials and higher investment costs. However, operating costs for energy consumption and maintenance may be lower throughout the life cycle of adaptive building envelopes and are rarely considered by designers and clients (Attia et al., 2018; Loonen, Trčka, Cóstola, & Hensen, 2013). Another reason is a lack of evidence in real-world applications of the benefits that can arise from these technologies or the lack of benchmarks, standards and testing procedures for evaluating adaptive building envelope performance (Hensen, Loonen, Archontiki, & Kanellis, 2015). The latter is in part attributed to uncertainty in predictions of adaptive building envelope performance when using existing building performance simulation (BPS) tools. BPS tools are software tools for predicting building performance by dynamically solving a set of mathematical equations. The main barriers to an accurate performance prediction of adaptive building envelopes in BPS tools are: (i) the limited modelling capabilities of existing BPS tools in simulating different types and ranges of control algorithms, on which the performance of adaptive building envelopes during operation largely depends (Loonen et al., 2017), (ii) the limited integration of multi-domain influences (Tabadkani, Tsangrassoulis, Roetzel, & Li, 2020) and (iii) the lack of occupant behaviour models that can successfully estimate the impact of users (Luna-Navarro, Gaetani, Anselmo, Law, & Overend, 2021). This limits the capability of BPS tools to adequately capture the influence of the control algorithm on the dynamic behaviour of adaptive building envelopes, which in turn increases the uncertainty about accurately predicting adaptive building envelope performance.

Taveres-Cachat, Favoino, Loonen, & Goia (2021) suggest that the co-simulation of adaptive building envelope models is a valuable approach to overcome the limitations discussed above. Co-simulation stands for *cooperative simulation* and refers to the joint simulation of separate models developed in different tools. The models are executed in individual simulators and are allowed to cooperate (Hafner et al., 2012; Trčka, Wetter, & Hensen, 2009). While the tools communicate and synchronise outputs, such as variables or status information, at certain points in time, each tool independently solves one part of the coupled problem between the communication points. A particular challenge in co-simulation is the time synchronisation and orchestration of the heterogeneous models and their individual solvers. To enable synchronisation and interactions across sub-simulators, co-simulation uses a coordinator-worker concept. The worker simulates sub-problems, and the coordinator initiates the start of the simulation and is responsible for coordinating the overall simulation and the data transfer between the tools (Broman et al., 2013). An earlier study by Borkowski, Donato, Zemella, Rovas, & Raslan (2019) proposed a modelling approach for the co-simulation of adaptive building envelopes. According to Attia, Hensen, Beltrán, & De Herde (2012), BPS tools should provide the flexibility to integrate guidance to influence design decisions, e.g. through optimisation of design solutions. However, many BPS tools lack such capabilities, and the modelling approach by Borkowski et al. (2019) integrates additional functionalities, such as optimisation, to support the design decision-making process.

It is still unclear whether co-simulation tools can accurately predict the thermal performance of adaptive building envelopes, albeit accurate adaptive building envelope models are crucial (Loonen et al., 2017). The accuracy of BPS tools is usually systematically tested through diagnostic methods, such as the Building Energy Simulation Test method, which allows comparison of the predictions of BPS tools with analytical solutions (Neymark et al., 2002). However, it is generally difficult to establish a common diagnostic method for co-simulation setups, as there is no one-size-fits-all approach to co-simulation, with the end product often being case-dependent (Trčka et al., 2009).

Despite the importance of assessing the accuracy of co-simulation setups for adaptive building envelopes, there is currently only one study that shows the empirical validation of a co-simulation setup for adaptive building envelopes, and that is a study by Taveres-Cachat & Goia (2020). In this study, a fully controlled test facility was used to validate a co-simulation setup for predicting the thermal and daylighting performance of a highly flexible parametric model of an external louvred shading system. The study by Taveres-Cachat & Goia (2020) does not take into account that the end products of co-simulation setups are very different and strongly depend on the respective co-simulation task. For example, they can differ depending on the internal routines of the tools used or the degree of complexity required to describe the task. This case dependency means that an approach for the validation of co-simulation of adaptive building envelopes is required that can be used for the different co-simulation setups. Therefore, the aim of the present study is to provide new evidence on how to validate co-simulation setups for thermal and control models of adaptive building envelopes. Since access to expensive calorimetric test facilities is often a barrier to providing empirical evidence for co-simulation setups, a full-scale non-calorimetric test facility was used. In addition, the approach by Tavares-Cachat & Goia (2020) has been extended through the use of an in-situ characterisation and a sensitivity analysis (SA), and details of each step of the assessment framework are provided for modellers from the façade design and engineering community to determine the accuracy of their own co-simulation setups.

To achieve these objectives, the present study adopted a twofold validation technique. On the one hand, empirical validation, which compares the outcomes of a tool with measured data, was used to test the solution process and appropriateness of the modelling approach within (i) its domain of applicability (Sargent, 2013) and (ii) the range of experimental uncertainty (Coakley, Raftery, & Keane, 2014). On the other hand, comparative testing, which compares the outcomes of a tool with the outcomes of another tool, was used to identify and diagnose sources of error or inaccuracy in the modelling approach. However, conducting comparative testing, which requires the use of a tool commonly accepted to represent the state-of-the-art, was complicated by the challenging representation of control algorithms for adaptive building envelopes in existing BPS tools. To still be able to perform comparative testing, only control algorithms that could be modelled in existing BPS tools were used in the present study.

The remaining part of the paper proceeds as follows: the next section (Section 2) provides an overview of the challenges of using non-controlled real-world facilities, such as MATELab, an outdoor test cell for occupant-façade interaction in the United Kingdom (UK) (Luna-Navarro & Overend, 2021), to empirically validate co-simulation setups. MATELab is a 30.0 m^2 office-like test facility designed to investigate occupant responses to different adaptive building envelope technologies. It has a modular glazed building envelope oriented to the east, south and west for testing different building envelope bays per orientation (Figure 2). Each bay has a maximum dimension of 1.5 m by 2.3 m and was designed to be easily installed and replaced, thereby allowing different building envelope technologies to be investigated in a relatively short period of time. In addition, each of the bays can be covered with obscuring cover panels made of highly insulated external and corresponding

internal plasterboard to generate a broad range of glazing orientation scenarios. Section 3 describes the co-simulation setup that is empirically validated and the assessment framework adopted for its validation. The results of the validation are then reported in Section 4 and discussed in Section 5.

2 CHALLENGES OF ADOPTING NON-CONTROLLED TEST FACILITIES FOR EMPIRICAL VALIDATION OF ADAPTIVE BUILDING ENVELOPE CO-SIMULATION MODELS

The thermal performance of building envelopes is usually measured in indoor calorimetric facilities, as the British Standards Institution describes in BS ISO 19467 (BSI, 2017b). In recent years, the performance of adaptive building envelopes has been increasingly tested in outdoor test facilities (e.g. Cattarin, Causone, Kindinis, & Pagliano, 2016). However, since they do not present full control of environmental parameters or calorimetric conditions, the thermal performance of these test facilities tends to be less accurate and controlled than traditional outdoor test cells for adaptive building envelopes.

Compared to real buildings, the modelling and calibration of not fully controlled outdoor test cells share some challenges but also bring benefits (Cattarin et al., 2016). Of key importance are the challenges discussed hereafter. The first challenge is that boundary conditions, thermal bridges and air infiltrations have a larger impact on the performance, given the smaller size of these test cells. In this sense, the detection of individual heat transfer paths is required, as recommended by Annex 58 of the International Energy Agency's Energy in Buildings and Communities (IEA EBC) programme (Roels, 2012). Thermal bridges and air infiltration rates also tend to be non-negligible due to the large surface-to-volume ratio.

The second challenge is the measurement and modelling of boundary conditions, which is particularly important as boundary conditions are not fully controlled. Monitoring and modelling of weather conditions are also important, especially the fraction of direct, diffuse and ground-reflected solar radiation (Judkoff & Neymark, 2006). Solar gains can have a large impact due to the larger surface of the transparent envelope relative to the total volume. The heat transfer coefficient of the surface must therefore be accurately selected from the large number of available empirical correlations to better describe the specific boundary conditions, such as wind velocity in the proximity of the building envelope (Moinard & G.Guyon, 1999).

If the thermal inertia of the building envelope is low, a third challenge is the unwanted oscillations in indoor air temperature compared to highly controlled test cells. Loutzenhiser et al. (2007) highlighted that predictions of cooling performance obtained through simulations are more sensitive to boundary conditions when performed on lightweight buildings compared to massive buildings due to the low thermal mass (and time constant) of the former case.

Lastly, real-world non-controlled test facilities typically include building automation systems for controlling heating, cooling, ventilation, lighting or window systems. These building automation systems usually have sensors, but they are not easily accessible or programmable to take measurements with the accuracy or frequency required for the calibration process of a BPS tool (Saelens & Reynders, 2016).

3 CO-SIMULATION SETUP AND ASSESSMENT FRAMEWORK FOR VALIDATION IN A NON-CONTROLLED TEST FACILITY

This section provides an overview of the co-simulation setup and the assessment framework used to validate it.

3.1 CO-SIMULATION SETUP

The co-simulation setup used the modelling approach developed by Borkowski et al. (2019) to model the blind automation system of MATELab. The modelling approach was specifically developed to accurately predict the thermal performance of control algorithms for adaptive building envelopes. To represent adaptive building envelopes, the modelling approach uses the following software:

- *EnergyPlus:* Integration of EnergyPlus v8.9.0 (National Renewable Energy Laboratory, 2018) to create the thermal model of the building and the building envelope.
- *Dymola:* Integration of Dymola v2020x (Dassault Systèmes, 2018), a commercial simulation programme based on the object-oriented, multi-domain modelling language Modelica (Modelica Association, 2017), to create the model of the control algorithm.
- *FMI Standard:* Integration of the Functional Mock-up Interface (FMI) Standard v2.0 (MODELISAR, 2014), an open middleware developed to facilitate communication and information exchange in co-simulation setups, to exchange information at each simulation timestep between EnergyPlus and Dymola.

Dymola is used as a coordinator simulation tool, and EnergyPlus as a worker simulation tool, as shown in Figure 1. This means that the EnergyPlus model is encapsulated and shared as a Functional Mock-up Unit (FMU) for co-simulation, which enables EnergyPlus to exchange information at each timestep with Dymola. The software package EnergyPlusToFMU v3.0.0 (Nouidui, Lorenzetti, & Wetter, 2020) is invoked to create the FMU, which is then manually imported into Dymola, the co-simulation coordinator, and connected to the control algorithm model. In the present study, the solar irradiance was measured in MATELab and provided as an input to the model to compute the blind position, which was then provided as an input for the FMU.

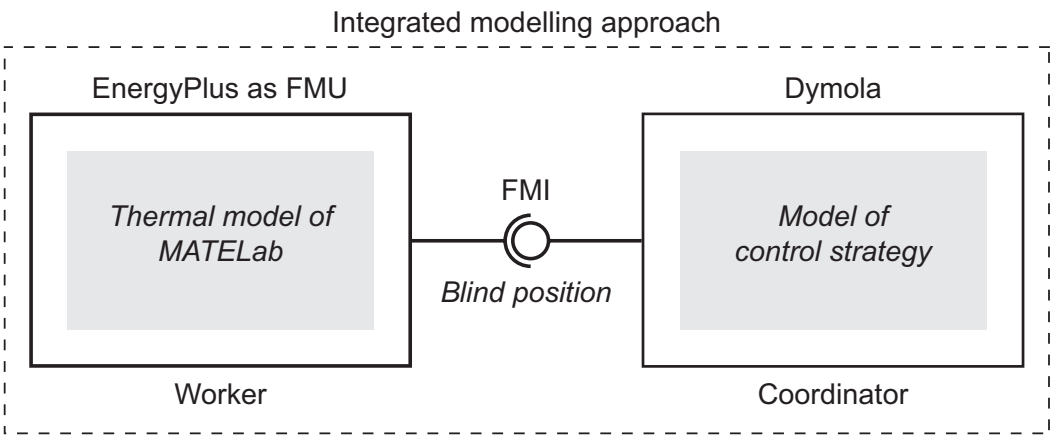

FIG. 1 Schematic of the co-simulation process: the control algorithm for the blind automation system in Dymola was coupled to the model of MATELab through the FMI Standard for information exchange at each zone timestep.

The co-simulation was automated through a script written in Python v3.8.5 (Python Software Foundation, 2020), which covered three basic steps: (i) export of the thermal model of MATELab as an FMU to be used in the co-simulation setup by calling EnergyPlusToFMU through the *Subprocess.call()* function; (ii) co-simulation of the entire model of MATELab through the *Simulator.simulate()* function of the BuildingsPy package (Lawrence Berkeley National Laboratory, 2019) and (iii) extraction and storage of data in CSV format for analysis. All simulations required for the validation were performed using the standard Dassl solver of Dymola with the default solver tolerance of 10^{-4} on a 2015 MacBook Pro with a dual-core Intel Core i5 processor of 2.7 GHz and with 16 GB of memory running Ubuntu 20.04 in a virtual machine.

3.2 ASSESSMENT FRAMEWORK

Table 1 describes the assessment framework to validate co-simulation setups for adaptive building envelopes used in non-controlled calorimetric test facilities. MATELab was chosen as a case study for a non-controlled and non-calorimetric test facility to collect the empirical data. The following sections describe the actions taken in each step of the framework's application and the rationale for the specific procedures and techniques used to identify, collect and analyse information.

TABLE 1 **Steps involved in the validation of co-simulation setups for control algorithms of adaptive building envelopes**

Step	
1	Definition of the validation scenario according to the purpose of the present study.
2	In-situ characterisation of the thermal properties of the validation scenario.
3	Collection of empirical data for the validation.
4	Creation of a reduced-complexity thermal model of the validation scenario in EnergyPlus based on the available facility construction documentation and the in-situ characterisation results.
5	Undertaking of a SA to identify key input variables for the calibration.
6	Calibration of the reduced-complexity thermal model of the validation scenario.
7	Creation of an adaptive building envelope model in the co-simulation setup by extending the model from Step 6 with a control algorithm for the building envelope.
8	Validation of the co-simulation setup by comparing the predicted data with the experimental data and identification of potential sources of error.

3.3 VALIDATION SCENARIO

The first step in the validation of the co-simulation setup was to define the validation scenario according to the purpose of the study. For the present study, MATELab was used with the east and west glazing panels covered with the obscuring cover panels internally and externally, thereby generating a south-facing glazed building envelope scenario. The south-oriented glazing consisted of two high-performance double-glazed units and internal automated Venetian blinds, as shown in Figure 3. This setup resulted in a window-to-wall ratio of approximately 0.5 on the south-oriented building envelope. The validation scenario's characteristics are reported in Appendix A.

a b

FIG. 2 Exterior views of MATELab: a. View of the south-west building envelope; b. View of the east building envelope with cover panels.

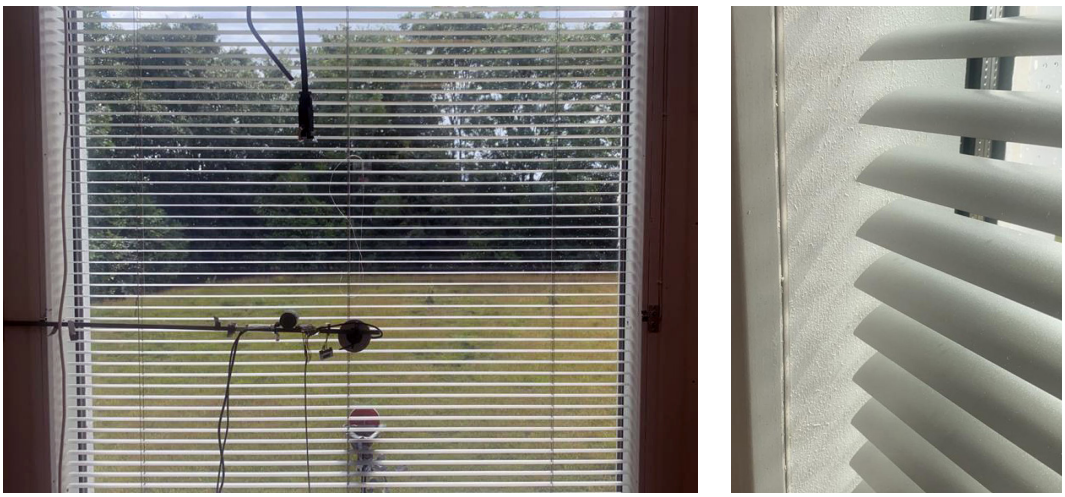

a b

FIG. 3 Views of blind installed in MATELab: a. View from inside to outside through blind with installed sensors; b. Detailed view of blind slats.

MATELab was unoccupied and operated in a free-running mode during this study, i.e. the underfloor air distribution (UFAD) system was switched off. This eliminated uncertainties arising from occupant behaviour and operation of the heating, ventilation and air-conditioning (HVAC) system, as suggested by previous work (Lomas, Eppel, Martin, & Bloomfield, 1997). It resulted in a simpler and more controlled validation scenario and facilitated the identification of inaccuracy or error in the building envelope and in the basic setup of the model.

Table 2 shows the control algorithm of the automated Venetian blinds that was implemented for the validation of the co-simulation setup. It was a rule-based control algorithm whose input and output were the solar irradiance, the time delay and the position of the blind.

TABLE 2 **Control algorithm for MATELab's blind automation system**

Input	$I_{sol,sky}$: global horizontal solar irradiance in W/m^2
Output	$I_{sol,south}$: global vertical solar irradiance on south surface in W/m^2

Algorithm	set I_{sol} = 1/3 x $I_{sol,sky}$ + 1.0 x $I_{sol,south}$
	if I_{sol} > 250 W/m^2 and t > 15 min then
	u_{blind} = 1.0
	else
	u_{blind} = 0.0
	end if

Due to the challenges of modelling a test facility such as MATELab, it was initially necessary to model a reduced-complexity model of MATELab, i.e. the thermal model with a static building envelope, allowing for a better understanding of the model dynamics. Accordingly, for the reduced-complexity model (Step 4), the blind automation system was turned off, so the building envelope was static. In addition, the blinds remained down all the time to minimise solar gain effects. In contrast, in the co-simulation model (Step 7), the blind automation system was turned on, so the building envelope was adaptive. Details of both models are reported in Table 3.

TABLE 3 **Building envelope setup of models in validation scenario**

Step	Model	Mode of operation	Position of blinds	Measurement period
4	Reduced-complexity model	Static	Down	14-21 May 2020
5	Co-simulation model	Adaptive	Alternating depending on control algorithm	8-16 August 2020

3.4 IN-SITU CHARACTERISATION OF THERMAL CHARACTERISTICS

In the second step, the thermal characteristics of the validation scenario were characterised. The thermal performance of the building envelope is often considered a major source of uncertainty in thermal building models, as the actual performance may differ from the performance estimated during design. For this reason, this methodology proposed the characterisation of the building envelope through in-situ measurements. The in-situ characterisation included the evaluation of the most important thermal properties of the building envelope: the thermal transmittance and the solar factor of the glass façade, the thermal bridges and the air infiltration flow rate. Further details of the calculations and procedures are given in Appendix B.

3.4.1 In-situ measurements of U- and g-values

According to ISO Standard 13790 (International Organization for Standardization Technical Committee 163/SC 2, 2008), the thermal characterisation of the building envelope is done by evaluating the air tightness, as recommended in BS EN 13829 (BSI, 2001), and by measuring two simplified parameters: (i) the thermal transmittance, i.e. the U-value (W/m^{2}K), and, if glazed, the solar factor, i.e. the g-value (-). These two parameters are usually measured under steady-state conditions either by laboratory tests or by software tools integrating databases of glass panes. However, due to the simplified approach in evaluating these parameters, they may not correspond to the actual thermal and solar performance (Goia & Serra, 2018). For example, there may be a discrepancy between the boundary conditions registered in situ and the standardised conditions

used during laboratory characterisation. Therefore, the simplified approach can lead to significant differences between the calculated and in-situ energy performance of the glazing system. Since there are no calorimetric conditions in non-controlled, non-calorimetric test facilities to assess the performance of the building envelopes, this framework used the in-situ characterisation based on the work by Goia and Serra (2018). The framework measures the U- and g-values through empirical measurements under non-calorimetric conditions. The measurements for the characterisation of the in-situ performance of the building envelope were taken as shown in Figure 4.

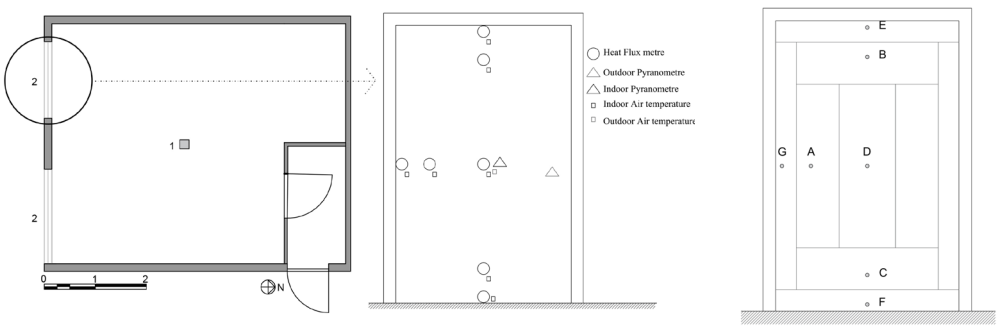

a *b*

FIG. 4 Experimental setup in MATELab: a. Plan view with the indoor sensors at the centre of the facility (1) and at the building envelope (2); b. Experimental setup at the building envelope with indication of the sensors used (sensor details are reported in Appendix B); c. Area-weighting for the calculation of the U-value..

3.4.2 Air tightness of building envelope

The air tightness of the building envelope can be characterised in situ by a blower door test (BDT) according to BS EN 13829 (BSI, 2001). This standard describes two types of test methods, depending on the purpose of the application. Method A (testing of a building in use) is applied during the heating or cooling season, while Method B (testing of the building envelope) assumes that intended openings in the building envelope are closed or sealed and the HVAC system is switched off. In a BDT, a specific range of pressure differences is created in the building envelope, and the airflow through the fan is monitored to assess the level of air tightness of the building envelope. Method B was chosen in this study since the goal of the air tightness test was to evaluate the performance of the building envelope. Therefore, all openings of the test facility were closed or sealed, including the air conditioning grills and vents, and the UFAD system was switched off. The indoor and outdoor temperatures were the same. The BDT was performed on a day when the meteorological wind speed was within the recommended range of BS EN 13829 (BSI, 2001).

After performing the BDT, the data were processed according to the Technical Memoranda TM23 by the Chartered Institution of Building Services Engineers (CIBSE, 2000) to determine the air tightness.

3.4.3 Thermal bridges assessment

If the validation scenario has a large ratio of external surface area to internal volume, thermal bridges can significantly affect the thermal model of the test facility and must be evaluated accordingly. Thermography provides a rapid and non-destructive means of assessing the thermal performance of building envelopes in situ (Asdrubali, Baldinelli, & Bianchi, 2012). Applications include (i) detection of missing or defective insulation, (ii) detection of air leaks and moisture and (iii) investigation of thermal discontinuities in the building envelope and thermal bridges. Thermographic tests should be carried out in accordance with BS EN 13187 (BSI, 1999) and BS EN ISO 6781-3 (BSI, 2015). When using thermography to identify thermal bridges, the temperature difference between the inside and outside of the building should be at least 10 °C. To minimise the effect of solar radiation on the results, in-situ thermographic tests are usually carried out during the night. In this study, the method proposed by Asdrubali et al. (2012) was used to quantify the effect of thermal bridges.

3.5 DATA COLLECTION PROCEDURES

The third step was to collect empirical data for the validation. During the measurement periods, the parameters described below were measured based on the available sensors for undertaking the model calibration and validation. After the data collection, the values were compiled and averaged over 1 minute. Details on the measurement campaign are reported in Appendix C.

3.5.1 Outdoor environmental parameters

Outdoor environmental parameters were needed to create the weather file for the validation of the model of MATELab. Weather data, specifically the dry bulb air temperature and the global horizontal solar irradiance, were collected using the weather station of MATELab, located on its roof at a height of approximately 3.0 m above ground level. It was assumed that these data were of particular importance for predicting MATELab's performance, in particular the aspects listed in Table 4.

TABLE 4 **Effects of measured outdoor environmental parameters on the performance of MATELab**

Parameter measured	Measurement instrument used	Performance aspects affected by parameter
Dry bulb air temperature	Weather station	Exterior surface convection Infiltration/ventilation sensible heat transfer
Global solar irradiance	Weather station	Fenestration heat gains Exterior surface heat balance Control algorithm

3.5.2 Indoor environmental parameters

Indoor environmental parameters were needed to assess the accuracy of the model during validation. The thermal performance indicator used was the indoor temperature, which was measured at the centre of the facility by a 1.0 m high sensing station (1 in Figure 4a).

3.5.3 Parameters related to control actions of blind automation system

Another data point required for the validation was the control actions of the blind automation system, namely the position of the blind. It was an important data point for the cross-validation of model outcomes, as the performance of adaptive building envelopes largely depends on the control algorithm during operation.

3.6 CREATION OF A REDUCED-COMPLEXITY THERMAL MODEL

The reduced-complexity thermal model was developed in the fourth step in EnergyPlus, which was chosen because it can represent the building envelope with sufficient accuracy (Attia et al., 2018). This offers the possibility to simulate and explore the performance of adaptive building envelope technologies constructed in MATELab in future studies. Furthermore, EnergyPlus allows the calculation of the thermal performance under non-stationary conditions, which is important in the present study as MATELab has a low thermal mass and is free-running. In the model, three thermal zones were implemented: (i) a supply air plenum under the raised floor, (ii) a return air plenum over the suspended ceiling and (iii) an occupied space. Further simulation parameters of the thermal model of MATELab are reported in Appendix D.

The models of the building envelopes were initially created based on the specifications received from the manufacturers of the building components. In a second iteration, the U- and g-values measured in Step 2 were incorporated. This was followed by a third iteration in which the U-values of the opaque building components were modified to capture the effects of the thermal bridges as measured in Step 2. Thermal bridges were included by increasing the conductivity of each building component by the corresponding value.

Data from outdoor environmental conditions were then used to create a new weather file for the study periods with Elements (Big Ladder Software & Rocky Mountain Institute, 2016), a free and open-source software tool for creating and editing custom weather files. Further details are reported in Appendix D.

3.7 SENSITIVITY ANALYSIS TO INFORM THE CALIBRATION

In the fifth step, a SA was carried out to identify key input variables for the calibration. The evaluation of the uncertainties is a fundamental step in the calibration process of BPS tools to confirm that a model was implemented correctly (de Wit & Augenbroe, 2002). In the present study, this was achieved by identifying and quantifying the degree of uncertainty of the most important input variables of the model of MATELab and then fine-tuning uncertain input variables to minimise discrepancies between measured and predicted data points. Possible sources of uncertainty in the model of MATELab are listed in Table 5.

TABLE 5 **Possible sources of uncertainty in the model of MATELab**

Type of uncertainty	Description
Specification uncertainty	Inaccurate or incomplete building and system specifications, such as geometry, material and blind properties and internal heat gains.
Modelling uncertainty	Simplifications and inaccurate assumptions of the physical processes, such as infiltration and ground heat transfer characteristics, in the computational simulation.
Numerical uncertainty	Errors introduced in the numerical analysis of the computational simulation.
Scenario uncertainty	Inaccurate representation of external conditions imposed on the building, such as climate conditions and occupant behaviour.

Detailed audits and in-situ characterisation are effective instruments to reduce the first source of uncertainty and should be carried out where possible. This includes in-situ measurements of actual geometrical characteristics as well as HVAC and lighting systems and schedules. Such in-situ characterisations are relatively easy to perform in outdoor test facilities that are not fully controlled (as described in Step 1), so that uncertainties due to inaccurate or incomplete building specifications become negligible.

To determine the most important input variables, the next step of the calibration process consisted of undertaking a SA (Chong and Menberg 2018). In this study, a global approach to SA was adopted, taking into account the interactions between variables by varying input variables simultaneously over the whole input sample space. The approach to global SA adopted was a Monte Carlo sensitivity analysis (MCSA), a variance-based method that measures the sensitivity of the output to the input variable by the amount of variance in the output caused by that input (Tian, 2013). It uses random samples from a given distribution, and this study selected the Latin hypercube sampling (LHS) method to generate the sample due to its efficient stratification properties. Figure 5 shows the schematic of the processes involved in the MCSA.

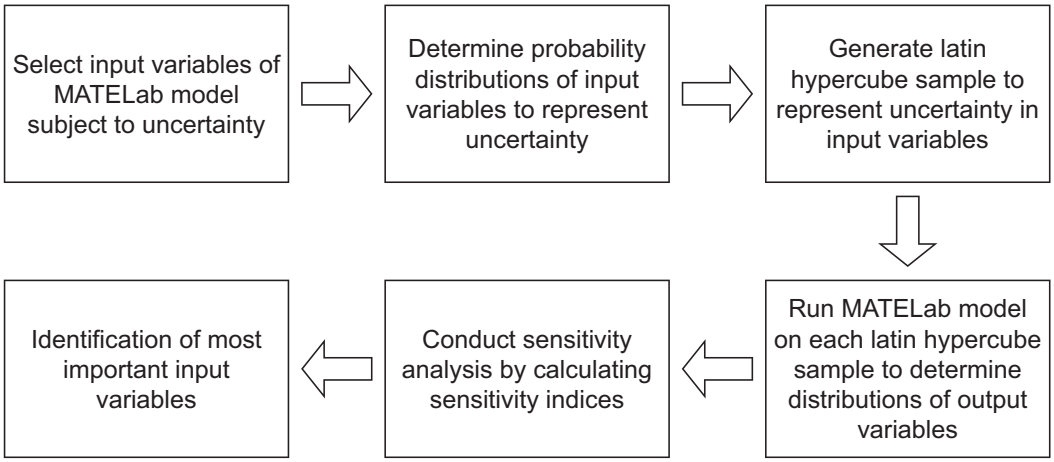

FIG. 5 Workflow diagram showing the processes involved in the MCSA.

In the MCSA, numerous sets of input-output variables were generated by running the model of MATELab on the input sample. The uncertain inputs considered in the MCSA are listed in Appendix E. Correlation-based methods were then applied to measure the strength of the input and output variables and to rank the input variables from 1 (the most important variables) to 8 (the least important variable). The two indices applied were: (i) the Pearson correlation coefficient (S_{Pear}) to measure the strength of the linear relationship between each of the input variables and the indoor temperature and (ii) the Spearman rank-order correlation coefficient (S_{Spear}) to measure the strength of the monotonic relationship between each of the input variables and the indoor temperature. Both indices had to be applied to capture information in the case of a non-linear relationship between input and output variables. The ranking was then used to generate plots for an initial qualitative evaluation of key input variables using the Python package Matplotlib (Hunter, 2007): (i) tornado plots to compare the relative importance of the input variables and (ii) scatter plots to show the relationships between the variables.

Given that sensitivity indices are estimated based on a limited sample, SA methods are subject to uncertainty (Yang, 2011). To get good estimations nonetheless, Monte Carlo simulations require many iterations depending on the complexity of the model and the number of parameters. The present work used the bootstrap technique (Yang, 2011), plotting the estimated statistic against the gradually increasing base sample size. Convergence is assumed as soon as there is no significant variation for each sensitivity index.

As the MCSA required many iterations and thus a lot of computing power, a research computing cluster was used to run the MCSA, which was completely automated through a Python script. To keep the computational time as short as possible, the MCSA only utilised the previously created reduced-complexity model. This required the use of EnergyPlus alone, which helped to reduce the computational intensity of the MCSA.

3.8 CALIBRATION OF A REDUCED-COMPLEXITY THERMAL MODEL

The reduced-complexity model was calibrated in the sixth step. Previous work on model calibration of outdoor test facilities suggested using an uncertainty analysis (UA) in the calibration of a thermal model (Jensen, 1995). An UA was described as 'the process of determining the degree of confidence in the true value when using a measurement procedure(s) and/or calculation(s)' by the American Society of Heating, Refrigerating and Air-Conditioning Engineers (ASHRAE, 2014, p. 10). It measures the acceptable level of model accuracy using uncertainty indices. The index applied in this part of the study was the coefficient of variation of root mean square error (CV-RMSE) index, which measures the variability of the errors between measured and simulated data points, thereby indicating the model's ability to fit the data

$$\mathrm{CV-RMSE}=\frac{1}{\overline{m}}\sqrt{\frac{\sum_{i=1}^{n}\left(m_{\mathrm{i}}-s_{\mathrm{i}}\right)^{2}}{n-p}}\times 100$$

Equation 1

where $\overline{m}$ is the average of the measured data points, *mi* is the measured data point for each model instance *i*, *si* is the simulated data point for each model instance *i*. *n* is the number of measured data points, and *p* is the number of adjustable data points, which is suggested to be zero for a calibration.

The IEA EBC Annex 58 developed a comprehensive framework and guidelines for reliable in-situ dynamic testing to characterise the actual energy performance of building components and whole buildings (Roels, 2012). This study applied the framework proposed in IEA EBC Annex 58 by using an automated method to calibrate the model once the experimental data collection has been performed. The automated calibration was implemented by using jEPlus (Zhang, 2012), a parametric tool for EnergyPlus, and an automated optimisation script in Python. It calculated the CV-RMSE index for each design option and selected the minimum CV-RMSE index as the final calibration solution. The parameters for the calibration were selected based on the results of the MCSA.

ASHRAE and other organisations (e.g. ASHRAE, 2014; Federal Energy Management Program, 2008; International Organization for Standardization Technical Committee 163/SC 2, 2008) specify

the maximum values for model calibration depending on whether the model was calibrated with hourly or monthly data. Furthermore, it should be noted that current calibration criteria only refer to the predicted energy consumption and do not account for uncertainties or inaccuracies of input parameters or the accuracy of the simulated environment (e.g. temperature profiles). This study used the hourly CV-RMSE index, which should be less than 30.0% for a model considered calibrated (ASHRAE, 2014). In previous work, calibrated models of outdoor test facilities have achieved low CV-RMSE values, such as 2.0% (Taveres-Cachat & Goia, 2020) or 3.4% (Martínez, Erkoreka, Eguía, Granada, & Febrero, 2019).

3.9 CREATION OF CONTROLLER MODELS

To model alternative dynamic controls of the adaptive building envelope, the previously created EnergyPlus model of MATELab was connected to a controller model in the seventh step.
The controller model was developed in (i) the Energy Management System (EMS) feature of EnergyPlus and (ii) Dymola in the co-simulation setup. The controller model in the EMS feature was used (i) for the SA and (ii) to generate outputs of a tool that is generally accepted as state-of-the art to identify and diagnose sources of error or inaccuracy in the co-simulation setup (Neymark et al., 2002). The co-simulation model was then used to test the accuracy of the adaptive building envelope model's predictions coupled with the modelling approach, a co-simulation setup developed in previous work.

3.9.1 Controller model in EMS feature of EnergyPlus

The EMS feature uses the EnergyPlus runtime language (Erl), a simple scripting language, to describe control algorithms (DOE 2018). EnergyPlus interprets and executes the control sequence implemented in Erl as the model is being run. In the present study, the EMS feature was used to provide high-level supervisory control to override the *WindowProperty:ShadingControl* object in EnergyPlus. Without the EMS feature, MATELab's control algorithm could only have been modelled in fragments, as blind control algorithms within EnergyPlus are either preset or time-scheduled. This might have had a negative impact on the model outcome (BSI, 2017a). To model a control algorithm that is based on boundary conditions or simulation state variables instead, the EMS feature must be used. Even though two aspects of the control algorithm were particularly complex to model in the EMS feature (Appendix D), it was implemented in the *EnergyManagementSystem:Program* object in EnergyPlus, as shown in Figure 6.

```
EnergyManagementSystem:Program,
    setyblind,                !- Name
    SET solrad_log_1 = @TrendValue solrad_log 1,    !- Program Line 1
    SET solrad_log_2 = @TrendValue solrad_log 2,    !- Program Line 2
    SET solrad_log_3 = @TrendValue solrad_log 3,    !- Program Line 3
    SET solrad_log_4 = @TrendValue solrad_log 4,    !- Program Line 4
    SET blind_on = Shade_Status_Interior_Blind_On,    !- Program Line 5
    SET blind_off = Shade_Status_Off,    !- Program Line 6
    IF (solrad_log_1 >= 250) && (solrad_log_2 >= 250) && (solrad_log_3 >= 250),    !- Program Line 7
    SET yblind_left = blind_on,    !- Program Line 8
    SET yblind_right = blind_on,    !- Program Line 9
    ELSEIF (solrad_log_1< 250) && (solrad_log_2 < 250) && (solrad_log_3 < 250),    !- Program Line 10
    SET yblind_left = blind_off,    !- Program Line 11
    SET yblind_right = blind_off,    !- Program Line 12
    ENDIF;                    !- Program Line 13
```

FIG. 6 Control algorithm for MATELab's blind automation system in the EMS feature of EnergyPlus.

3.9.2 Controller model in co-simulation setup

To link the EnergyPlus model to the Dymola model, the external interface of EnergyPlus had to be activated. With the *ExternalInterface* object present, the values listed in the object received their inputs from the FMI Standard at each zone timestep. The software package EnergyPlusToFMU was used to export the EnergyPlus model of MATELab as an FMU for co-simulation. The FMU was then imported into Dymola, where it appeared as an input/output block and was connected to the controller model. Figure 7 represents the model of the control algorithm in Dymola, with (i) the input data of the monitored solar irradiance, (ii) the control algorithm and (iii) the FMU.

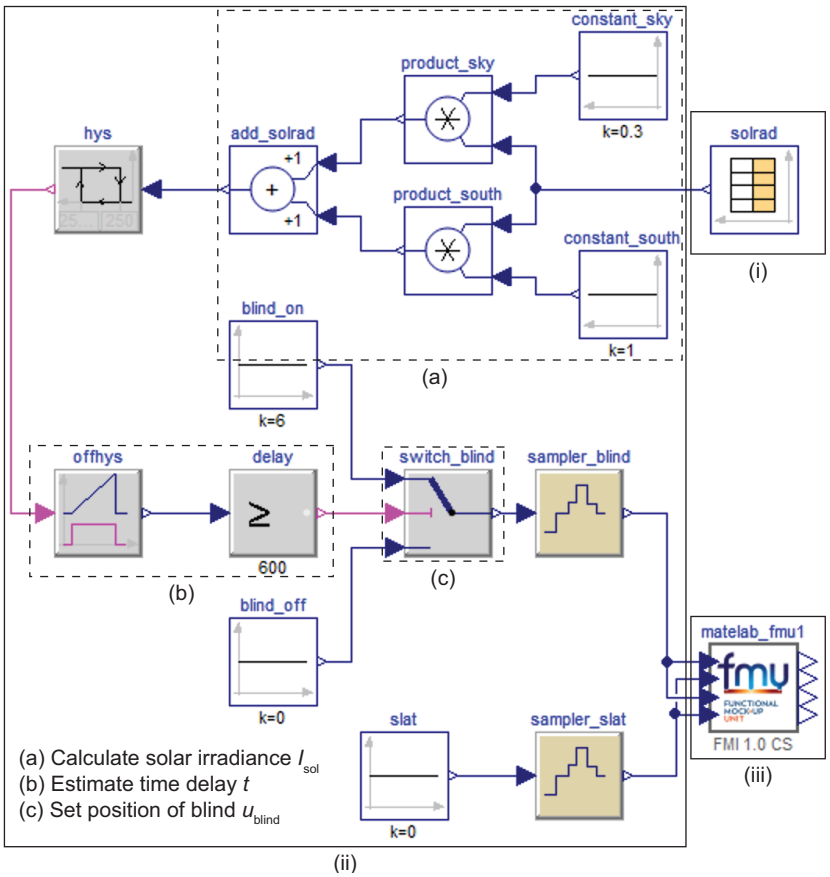

FIG. 7 Graphical representation of the control algorithm model for MATELab's blind automation system in Dymola.

3.10 ANALYSIS OF VALIDATION RESULTS

When analysing the validation results in the eighth step, there could be large discrepancies between measured and simulation-predicted data points. Another UA was therefore carried out to quantify how well the model of MATELab described the variability in the measured data, hence decreasing the model's uncertainty and increasing the level of confidence in it. The uncertainty indices used in this part of the study to evaluate the accuracy were the normalised mean bias error (NMBE) and the CV-RMSE (as in Step 6, see Section 3.6.2). The NMBE index gives the global difference between measured and simulated data points by normalising the average of the errors of a sample space and dividing it by the mean of the measured data points ($\overline{m}$).

$$\mathrm{NMBE} = \frac{1}{\overline{m}} \times \frac{\sum_{i=1}^{n} \left(m_i - s_i \right)}{n - p} \times 100$$

Equation 2

where *mi* is the measured data point for each model instance *I*, *si* is the simulated data point for each model instance *i*, and *n* is the number of measured data points. *p* is the number of adjustable data points, which is suggested to be zero for the validation.

Although the NMBE index is a good measure of model accuracy, its main problem is the cancellation error, where the sum of positive and negative values reduces the value of the NMBE index (Ruiz & Bandera, 2017). Consequently, using this index alone is not recommended, and the CV-RMSE index was used as a further measure of model accuracy.

As outlined in Figure 8, an iterative process was applied to reduce discrepancies between measured and predicted data points. The model's output variable of interest used to calculate the uncertainty indices was the indoor temperature, and the acceptable range of accuracy should be in accordance with ASHRAE Guideline 14-2014 (ASHRAE, 2014). According to the guideline, the hourly NMBE index is required to be less than 10.0%, and the hourly CV-RMSE index less than 30.0% to evaluate a model as validated.

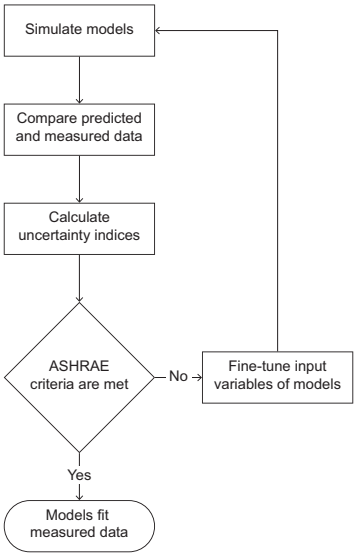

FIG. 8 Iterative process for the reduction of discrepancies between measured and predicted data.

4 RESULTS AND DISCUSSION

This section discusses the results that emerged from this study. It begins by presenting the results related to the in-situ measurements and the results of the MCSA. It then moves on to analyse the calibration of the reduced-complexity model of MATELab and the validation of the co-simulation model of MATELab.

4.1 IN-SITU MEASUREMENTS

Figure 9a shows the linear regression leading to the determination of the in-situ thermal transmittance for the measurement points A, B, C and D given in Figure 4, while Figure 9b shows the linear regression leading to the evaluation of the U-values at the edge of the glass, corresponding to the measurement points E, F and G in Figure 4. The resulting U-values are reported in Table 15 in Appendix F. The total U-value was then evaluated by calculating a weighted average of each zone corresponding to the areas of influence in Figure 4. The total U-value was assessed as 1.2 W/Km^2, which is higher than the U-value of 1.1 W/Km^2 originally obtained from the manufacturer's specifications. The total U-value was adjusted accordingly in the model of the construction elements of the thermal model.

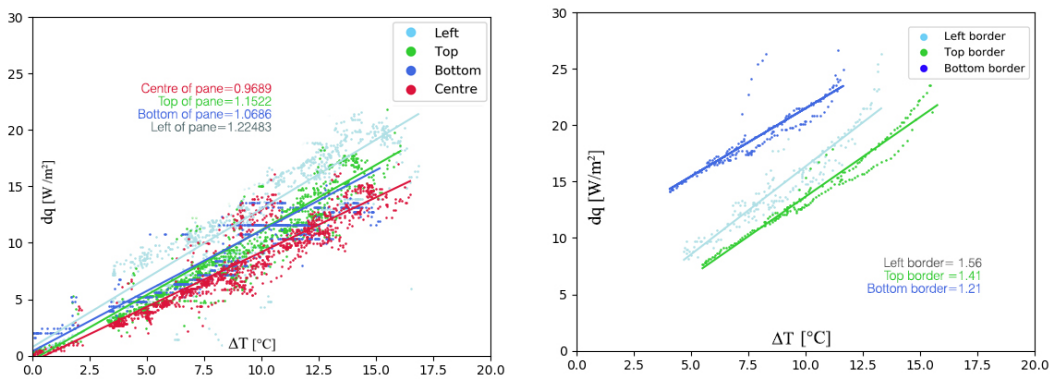

a b

FIG. 9 Results from the U-value monitoring: a. Linear regressions leading to the computing of the U-values closer to the centre of the glass pane; b. U-values at the edge of the glass pane.

Figure 10 shows the results of the g-value monitoring and the corresponding linear regression for the empirical evaluation of the g-value. It can be seen that the g-value of 0.4 is higher than the originally assumed 0.3 in the first iteration of the model. This was adjusted accordingly in the second iteration.

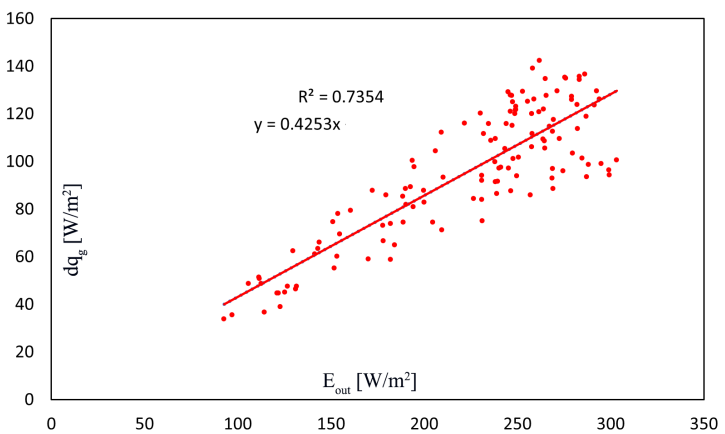

FIG. 10 Linear regression leading to the evaluation of the g-value.

The results of the BDT are shown in Figure 11, which plots the characteristic curve of the air infiltration in MATELab. The air permeability of the building envelope was found to be 2.3 air changes per hour at 50.0 Pa. This value is within the recommended maximum limit of the UK Part L regulation for fuel and power conservation (Office of the Deputy Prime Minister, 2006). The value of the flow coefficient *C* was determined to be 0.0084, which was then used as an input in the *ZoneInfiltration:FlowCoefficient* object in EnergyPlus. A schedule of 24/7 and a conventional pressure exponent of 0.7 were used. For the stack coefficient, the value recommended by ASHRAE Fundamentals for a one-storey building with a typical shelter for a rural house was used, corresponding to 0.000145 (ASHRAE, 2017).

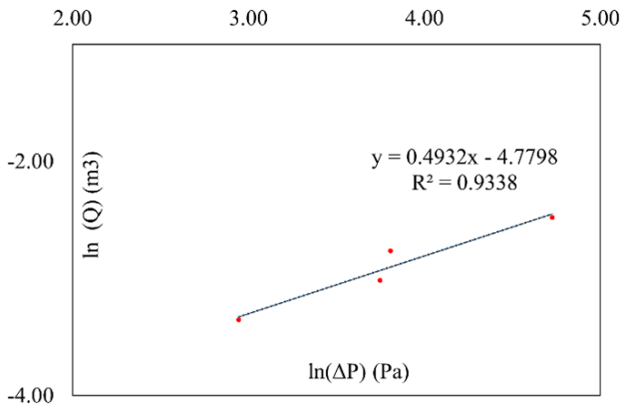

FIG. 11 Characteristic curve of the air infiltration of MATELab.

Finally, the thermal images in Figure 12 show the temperature distribution of the outdoor surface temperature of MATELab. The even colouring of the walls around the windows indicates a uniform installation of the thermal wall insulation. The temperature distribution also shows that there are no significant thermal bridges in the building envelope, except for the expected thermal bridges at the interface between two different materials (e.g. glass-frame) and at geometrical discontinuities.

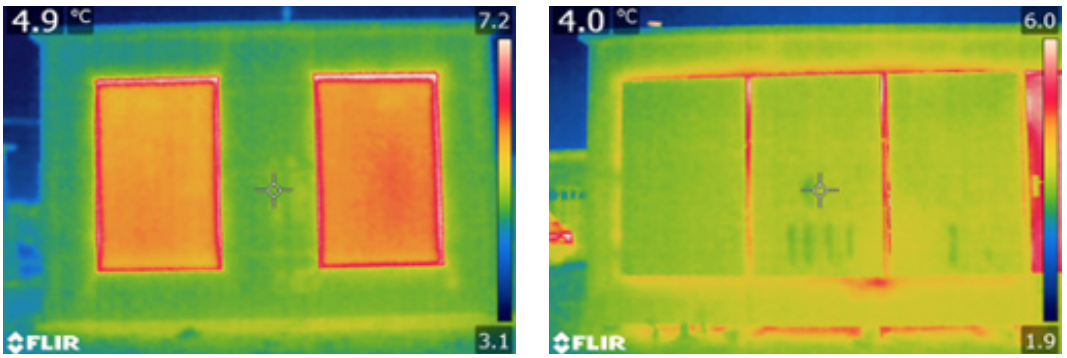

a *b*

FIG. 12 Thermographic images of two different building envelopes of MATELab, taken from the outside: a. South-facing glass façade; b. East building envelope with opaque covers on glass.

4.2 MONTE CARLO SENSITIVITY ANALYSIS

The aim of the MCSA was to determine the most important input variables in the validation scenario by using the sensitivity indices S_{Pear} and S_{Spear} to evaluate the relationships between the input variables and the indoor air temperature T_{ai}.

As discussed above, this study adopted the bootstrap technique to achieve convergence. S_{Pear} and S_{Spear} were plotted against the gradually increasing number of iterations N, and convergence was assumed as soon as there was no significant variation for each sensitivity index. Figure 13 shows that the indices reveal a clear distinction between the two most important input variables – the internal heat gains Q_{int} and the infiltration flow rate Q_{inf} – and the other six variables after a few hundred iterations (N = 750). Internal heat gains describe the heat emitted within MATELab from internal sources, especially computer equipment, resulting in a temperature increase within the facility, and infiltration describes the unintended flow of outside air into MATELab, typically caused by cracks in the building envelope.

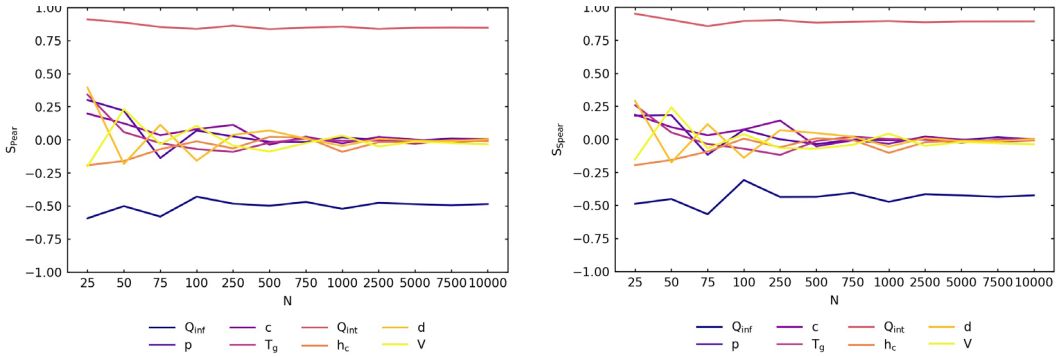

a b

FIG. 13 Convergence of S_{Pear} and S_{Spear} for input variables and increasing base sample size expressed as number of iterations N.

While the indices started to converge at the base sample size of around 5000, only the two most important variables (Q_{int} and Q_{inf}) could be identified with certainty. The other six variables (p, c, T_g, h_c, d and V) had no noticeable effect on the model outcome compared to the internal heat gains and the infiltration flow rate. The data show that these six variables had a negligible correlation with S_{Pear} and S_{Spear} close to zero. This indicated that the relationship was random or non-existent. It would thus have been computationally ineffective to increase the number of iterations further. As a consequence, convergence was assumed.

This study applied two correlation-based methods to measure the strength of the input and output variables. From the data in Figure 14, it is apparent, however, that S_{Pear} and S_{Spear} were similar for each of the input variables, consequently leading to the same conclusions. The data also shows that the two most important input variables in relation to the indoor air temperature were the internal heat gains Q_{int} and the infiltration flow rate Q_{inf}. Therefore, variations in the indoor air temperature could largely be attributed to variations in the internal heat gains and the infiltration flow rate, and the internal heat gains and the infiltration flow rate were used to calibrate the model.

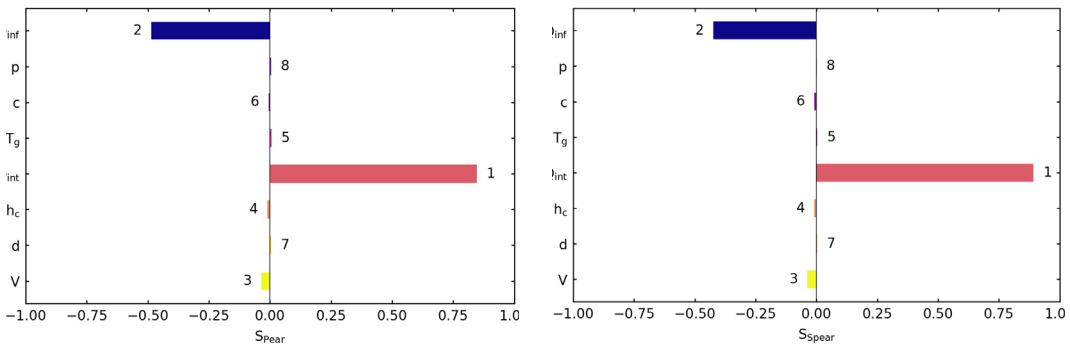

FIG. 14 Comparison of the relative importance of the input variables for N = 10000, with the rank of each input variable given next to the bar (1 is the highest rank).

4.3 CALIBRATION OF A REDUCED-COMPLEXITY THERMAL MODEL

The aim of calibrating the reduced-complexity model with the static building envelope was to minimise the error between the measured and predicted indoor air temperature T_{ai}. This was achieved by fitting the internal heat gains and the infiltration flow rate through the automated process described in Section 3.8. In this process, the model was calibrated by performing an automated parametric analysis and running 4,642 simulations varying the internal heat gains and the infiltration flow rate. The simulation scenario with the minimum CV-RMSE index was then selected, indicating a good model fit. Table 6 shows the CV-RMSE index and the correspondent internal heat gains and infiltration flow rate before calibration (predicted based on the construction documents and the results of the in-situ characterisation) and after calibration (predicted based on the results of the parametric analysis). Figure 15 compares the predicted indoor air temperature T_{ai} before and after calibration with the measured indoor air temperature. In addition, the following changes were made to the model:

- Since infiltration highly depends on outside wind conditions, measured wind data from MATELab's weather station were added to the weather file.
- Since MATELab's weather data were not measured at World Meteorological Organization standard conditions, the *Site:WeatherStation* object was added to EnergyPlus to specify the measurement conditions for the climatic data, such as the height above ground of the weather station.

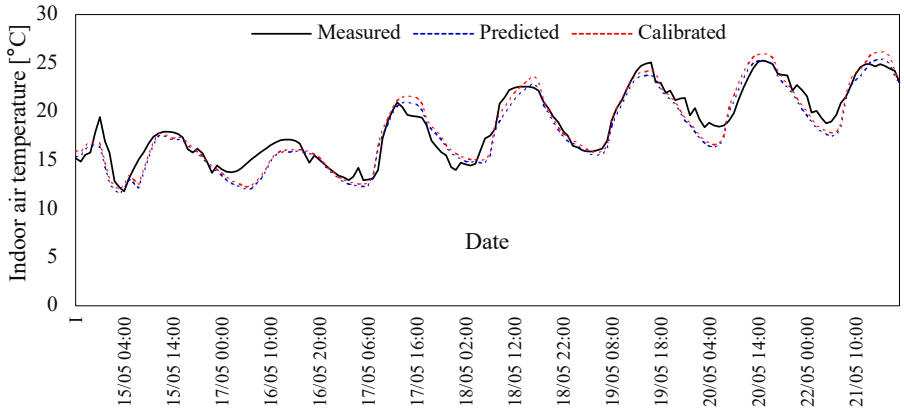

FIG. 15 Comparison of measured and predicted Tai before and after calibration of the reduced-complexity model.

TABLE 6 **Comparison of CV-RMSE index before and after calibration**

Model	CV-RMSE (%)	Q_{int} (W/m²)	Air infiltration
Before calibration	6.6	8.7	Q_{inf}: 0.0008 m³/s m²
After calibration	6.3	13.0	C: 0.0084

The results in this section indicate that the in-situ characterisation proved useful in improving the accuracy of the predicted data. This shows that including the non-calorimetric in-situ characterisation of the building envelope in the assessment framework may contribute to a more accurate prediction of the indoor air temperature. It should be noted that the original thermal model developed based on construction documents was already very accurate, with a CV-RMSE index of 6.6%, well below the ASHRAE requirement of 30.0%. The reason for this could be the authors' detailed knowledge of MATELab's construction details. The fact that the data collection was conducted shortly after the test facility was built may also have contributed to the accurate results, as the building components were largely unaffected by deterioration and maintenance factors. For example, the U-values were not significantly different from those published in the construction documents. Nevertheless, an in-situ characterisation is recommended in all cases because the performance of building components deteriorates over time. Therefore, it is important to measure their actual performance at the time of data collection. In addition, the use of non-stationary models to measure the actual performance of the building envelope may be considered.

4.4 VALIDATION OF A CO-SIMULATION MODEL OF MATELAB

The validation was undertaken to reduce the uncertainty of the model of MATELab created in a co-simulation setup. The control algorithm was modelled, in addition to Dymola, in the EMS scripting feature of EnergyPlus to identify and diagnose sources of error or inaccuracy in the co-simulation setup. Since the parameters of the thermal model and the weather file were identical for both models, the main difference between them was that the control algorithm was modelled in different tools. When comparing the predictions of the models of MATELab with the actual measured data, good agreement with the measured data was found. The data were analysed by descriptive statistics, and the summary statistics for the uncertainty indices NMBE and CV-RMSE are compared in Table 7. The data in the table shows that the NMBE minima (Dymola: -1.4%, EMS: -1.4%) and maxima (Dymola: 0.8%, EMS: 0.7%) were well below the ASHRAE requirement of 10.0% for hourly empirical data. With median values of -0.1% (Dymola) and -0.1% (EMS) for the NMBE indices, both Dymola and EMS models tended to slightly over-predict the measured data. However, NMBE indices close to zero indicate that there is only a small difference between the predicted and actual indoor air temperature and that the model has a sound goodness-of-fit. Similarly, the CV-RMSE minima (Dymola: 0.01%, EMS: 0.02%) and maxima (Dymola: 20.6%, EMS: 21.0%) were well below the AHREAE requirement of 30.0%, which was also suggestive of a good model fit.

TABLE 7 **Summary statistics of uncertainty indices applied in validation**

Type of error	Tool	Median	Standard deviation	Minimum	Maximum
NMBE (%)	Dymola	-0.1	0.5	-1.4	0.8
	EMS	-0.1	0.5	-1.4	0.7
CV-RMSE (%)	Dymola	6.3	4.0	0.01	20.6
	EMS	6.2	4.2	0.02	21.0

The results of the validation are also shown in Figure 16. When comparing the measured and predicted indoor air temperature data, the discrepancies between measured and predicted data become apparent, especially in the last three days when the weather quickly changed from sunny to cloudy. A possible explanation for this could be inaccuracies in the thermal mass (e.g. due to computer equipment inside MATELab). If the real test facility was lighter than the model, it gave back more thermal energy and cooled down faster when the environmental temperatures were cooler than the thermal mass.

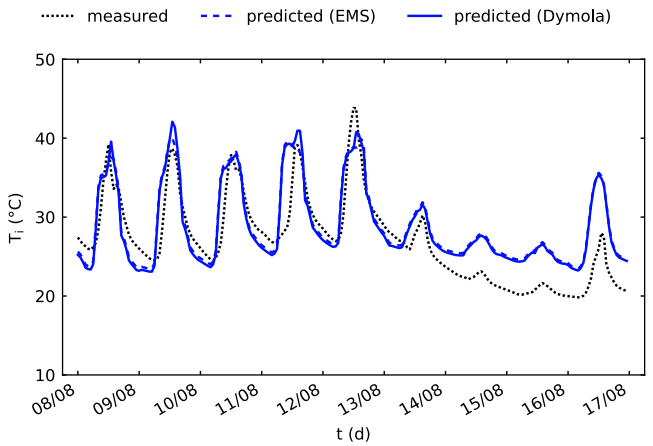

FIG. 16 Comparison of measured and predicted Tai in the validation of the co-simulation model.

Interestingly, Dymola and the EMS feature predicted slightly different outcomes. Since the weather file and the parameters of the thermal model were identical, it can be assumed that the differences were due to the different models and solution techniques supported by each of the tools used to represent the control algorithm. For example, the EMS feature used the Erl programming language commands, such as IF-ELSEIF-ELSE-ENDIF statements and trend variables, and Dymola used the Modelica Standard Library (Modelica Association, 2016) model components, such as *Modelica.Blocks.Logical.Hysteresis* and *Modelica.Blocks.Logical.Switch*. But such small discrepancies were expected and are in line with earlier observations, e.g. by Trcka, Wetter, and Hensen (2009).

These different approaches to representing the control algorithm in the respective tools may have resulted in differences in how the output of the control algorithm was computed. A differently computed control algorithm could then have led not only to discrepancies in the predictions of the blind movements but also to discrepancies in the predictions of the indoor temperatures. Figure 17 compares the measured and predicted blind positions for two representative days. On 11 August (Figure 17a), the blinds closed at 13:10 (measured), while in Dymola they moved at 13:15 and in the EMS feature at 13:05. This error could be linked to data averaging during the analysis according to the 5-minute timestep of the simulation, but also to an inaccurate implementation of the time delay in either the real test facility or in the models. Furthermore, the EMS feature predicted to open the blinds at 16:15 (measured: 15:55, Dymola: 16:00). This inaccuracy could be due to the input data of the monitored solar irradiance for the control algorithm, which contained 15-minute interval data and was provided to EnergyPlus using values from an external CSV file as a schedule. The input data in Dymola were the same as in EnergyPlus. But whereas Dymola was able to interpolate the data so that they matched the measured data, EnergyPlus did not interpolate them but adopted the same value for 15 minutes. After 15 minutes, EnergyPlus moved on to the next value in the input file and adopted this value again for a period of 15 minutes.

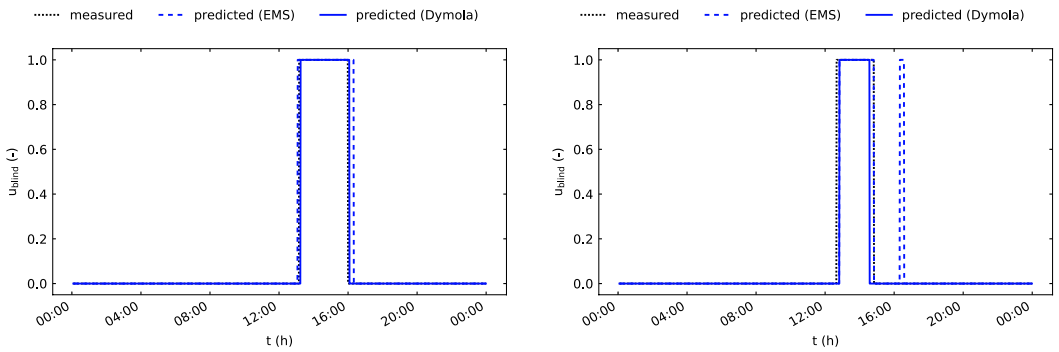

FIG. 17 Comparison of measured and predicted blind positions (0: blinds open, 1: blinds closed) for two representative days.

The blind behaviour discussed above also appeared on 12 August (Figure 17b). The EMS feature predicted a spike in the movement of the blinds for 15 minutes between 16:20 and 16:35. The reason for this was again the interpolation of the solar irradiance data. While there was one occurrence where the solar irradiance was greater than the control threshold of 250 W/m^2, the blinds should not have moved, given the 15-minute time delay. Because of the interpolation error described above, the control algorithm in the EMS feature assumed that the solar irradiance was above the threshold for more than 15 minutes, resulting in the blinds being incorrectly closed.

These results indicate that both Dymola and the EMS feature of EnergyPlus were able to represent the control algorithm for MATELab's blind automation system. But it remains unclear whether or not the differences between the predicted and measured blind behaviours were due to an inaccurate implementation of the time delay in the real test facility. Although such imperfect knowledge of the experimental objects being simulated is common (Judkoff and Neymark, 2006), it is recommended to fully understand the implementation of a control algorithm in the real test facility to be able to model it correctly. Also, the results may provide some advice to other modellers on how to adapt the setup of similar models:

- Even though EnergyPlus was set to interpolate the values from the 15-minute interval input data to the 5-minute simulation timestep, this study found that EnergyPlus did not correctly interpolate the input data, resulting in inaccurate predictions. Future work should take this error into account and debug the EnergyPlus model to thoroughly determine its cause(s).
- A potential solution to resolve this error could be to provide solar irradiation data at 5-minute intervals to EnergyPlus. In this case, EnergyPlus would not need to interpolate the input data so that it could correctly (i) calculate the time delay and (ii) predict the positions of the blinds.

5 CONCLUSION

This research was undertaken to provide new evidence on how to validate co-simulation setups for adaptive building envelopes using a full-scale non-controlled and non-calorimetric test facility. The adaptive component of the building envelope in the case of the present study was MATELab's blind automation system. The results show that the validated model of MATELab accurately captured the building envelope controls and properties with median CV-RMSE indices of 5.9% for Dymola in the co-simulation setup and 6.1% for the EMS feature. This underlines the capability of the proposed assessment framework to validate both models to accurately reflect the variability in the measured data. Furthermore, the result suggests that the co-simulation setup can generally be used to validate

the behaviour of adaptive building envelopes, confirming the findings of Taveres-Cachat et al. (2021), who found that their co-simulation setup with Grasshopper had a CV-RMSE index of 2.0%, also well within the acceptable range of accuracy.

Nevertheless, it may be difficult to generalise these results because, on the one hand, empirical validation only tests 'whether the simulation model's output behaviour has the accuracy required for the model's intended purpose over the domain of the model's intended applicability' (Sargent, 2013, p. 18). The co-simulation setup consequently validated the behaviour of MATELab only for its intended application (i.e. rule-based control algorithm). Further testing is hence required to create a truth standard for other control algorithms and to validate the co-simulation setup over the complete domain of its intended applicability. On the other hand, empirical validation should never be used as the only validation method due to measurement uncertainty and experimental complexity (Cattarin et al. 2018). Consequently, there is abundant room for further progress in fully determining the accuracy of the co-simulation setup, e.g. by undertaking inter-model comparisons.

Despite its lack of generalisation, the assessment framework can be used by modellers from the façade design and engineering community to determine the accuracy of their own co-simulation setups. To enable them to use the framework, it is important to provide the key lessons learned:

- During the first set of measurements, the HVAC system of MATELab was turned on. Very soon, it became clear that the data were too complicated and hindered the understanding of the effects of, for example, the building envelope, the heat gains and the climate conditions on the building dynamics. Therefore, it was decided to perform the validation with data from the free-running MATELab to determine the cause of certain deviations in the data.
- The initial simulation results, which considered the manufacturers' specifications for the building components, differed from the measurements. To ensure that key input values, such as the infiltration rate, were entered correctly, it was decided to perform an in-situ characterisation.
- It sometimes proved difficult to compare predicted with measured data and especially to find output variables in the thermal EnergyPlus model suitable for comparison with the measured sensor variables. While the authors of this study were fortunate to have full access to the sensor variables in MATELab, this could complicate the validation of adaptive building envelopes in other studies. It is therefore recommended to ensure that appropriate empirical data are available for validation.
- Despite the high number of input variables, the MCSA accelerated the investigation of the effects of the input variables on the outcome of the MATELab model. Therefore, the MCSA was particularly useful in reducing the number of parameters to be adjusted during the calibration process. However, since a high number of simulations was necessary to achieve convergence, the use of the reduced-complexity model appeared to be critical to potentially reduce the time needed to run the MCSA.

By ensuring that the predictions of the co-simulation setups of modellers from the façade community are accurate, the assessment framework has the potential to lead to broader use of co-simulation in the industry. Co-simulation is a valuable approach to overcoming the limitations in accurately predicting the performance of adaptive building envelopes in BPS tools. This, in turn, can help façade designers and engineers to reliably evaluate the performance of adaptive building envelopes and integrate them more easily into building projects. In turn, more adaptive building envelopes may lead to more energy-efficient buildings, which may help achieve global climate change goals.

CRediT author statement

Esther Borkowski: Conceptualization, Methodology, Software, Validation, Formal Analysis, Investigation, Resources, Data curation, Writing – Original Draft, Writing – Review & Editing, Visualization, Project administration

Alessandra Luna-Navarro: Conceptualization, Methodology, Software, Validation, Formal Analysis, Investigation, Resources, Data Curation, Writing – Original Draft, Writing – Review & Editing, Visualization, Project administration

Michalis Michael: Methodology, Formal Analysis, Investigation, Data Curation, Writing – Original Draft, Visualization

Mauro Overend: Writing – Review & Editing, Supervision

Dimitrios Rovas: Writing – Review & Editing, Supervision

Rokia Raslan: Writing – Review & Editing, Supervision

Acknowledgements

The authors acknowledge the use of the UCL Myriad High Throughput Computing Facility (Myriad@ UCL), and associated support services, in the completion of this work.

References

American Society of Heating, Refrigerating and Air-Conditioning Engineers. (2014). *ASHRAE Guideline 14-2014: Measurement of Energy and Demand Savings*. Atlanta, GA, USA: ASHRAE.

American Society of Heating, Refrigerating and Air-Conditioning Engineers. (2017). *2017 ASHRAE Handbook—Fundamentals (SI Edition)*. ASHRAE.

Asdrubali, F., Baldinelli, G., & Bianchi, F. (2012). A quantitative methodology to evaluate thermal bridges in buildings. *Applied Energy*, *97*, 365–373. https://doi.org/10.1016/j.apenergy.2011.12.054

Attia, S., Bilir, S., Safy, T., Struck, C., Loonen, R., & Goia, F. (2018). Current trends and future challenges in the performance assessment of adaptive façade systems. *Energy and Buildings*, *179*, 165–182. https://doi.org/10.1016/j.enbuild.2018.09.017

Attia, S., Hensen, J., Beltrán, L., & De Herde, A. (2012). Selection criteria for building performance simulation tools: Contrasting architects' and engineers' needs. *Journal of Building Performance Simulation*, *5*(3), 155–169. https://doi.org/10.1080/19401493.2010.549573

Big Ladder Software & Rocky Mountain Institute. (2016). *Elements*. Retrieved from https://bigladdersoftware.com/projects/elements/

Borkowski, E., Donato, M., Zemella, G., Rovas, D., & Raslan, R. (2019). Optimisation Of Controller Parameters For Adaptive Building Envelopes Through A Co-Simulation Interface: A Case Study. *Proceedings of Building Simulation 2019: 16th Conference of IBPSA*. Rome, Italy.

British Standards Institution. (1999). *BS EN 13187:1999: Thermal performance of buildings. Qualitative detection of thermal irregularities in building envelopes. Infrared method*. British Standards Institution. Retrieved from https://bsol.bsigroup.com/en/Bsol-Item-Detail-Page/?pid=000000000001569434

British Standards Institution. (2001). *BS EN 13829:2001: Thermal performance of buildings. Determination of air permeability of buildings. Fan pressurization method*. British Standards Institution. Retrieved from https://bsol.bsigroup.com/en/Bsol-Item-Detail-Page/?pid=000000000019983036

British Standards Institution. (2015). *BS EN ISO 6781-3:2015: Performance of buildings. Detection of heat, air and moisture irregularities in buildings by infrared methods. Qualifications of equipment operators, data analysts and report writers*. British Standards Institution. Retrieved from https://bsol.bsigroup.com/en/Bsol-Item-Detail-Page/?pid=000000000030259341

British Standards Institution. (2017a). *BS EN 15232-1:2017: Energy Performance of Buildings. Impact of Building Automation, Controls and Building Management. Modules M10-4,5,6,7,8,9,10*. British Standards Institution.

British Standards Institution. (2017b). *BS ISO 19467: 2017: Thermal performance of windows and doors. Determination of solar heat gain coefficient using solar simulator*. British Standards Institution. Retrieved from https://bsol.bsigroup.com/en/Bsol-Item-Detail-Page/?pid=000000000030294394

Broman, D., Brooks, C., Greenberg, L., Lee, E., Masin, M., Tripakis, S., & Wetter, M. (2013). Determinate composition of FMUs for co-simulation. *Proceedings of the International Conference on Embedded Software (EMSOFT)*, 1–12. Montréal, Canada: IEEE Press.

Cattarin, G., Causone, F., Kindinis, A., & Pagliano, L. (2016). Outdoor test cells for building envelope experimental characterisation – A literature review. *Renewable & Sustainable Energy Reviews*, *54*, 606–625. https://doi.org/10.1016/j.rser.2015.10.012

Chartered Institution of Building Services Engineers. (2000). *Testing Buildings for Air Leakage - CIBSE Technical Memoranda TM23: 2000*. Chartered Institution of Building Services Engineers.

Chartered Institution of Building Services Engineers. (2015). *CIBSE Guide A: Environmental design*. London, UK: Chartered Institution of Building Services Engineers.

Coakley, D., Raftery, P., & Keane, M. (2014). A review of methods to match building energy simulation models to measured data. *Renewable and Sustainable Energy Reviews*, *37*, 123–141. https://doi.org/10.1016/j.rser.2014.05.007

Dassault Systèmes. (2018). *Dymola*. Lund, Sweden. Retrieved from https://www.3ds.com/productsservices/catia/products/dymola

de Wit, S., & Augenbroe, G. (2002). Analysis of uncertainty in building design evaluations and its implications. *Energy and Buildings*, *34*(9), 951–958. https://doi.org/10.1016/S0378-7788(02)00070-1

Department of Energy. (2018). *EnergyPlus v9.0.1 Documentation—Application Guide for EMS*. Department of Energy.

Dervishi, S., & Mahdavi, A. (2012). Computing diffuse fraction of global horizontal solar radiation: A model comparison. *Solar Energy*, *86*(6), 1796–1802. https://doi.org/10.1016/j.solener.2012.03.008

Digital Technology Group. (n.d.). *DTG weather station*.

Duffie, J. A. (2013). *Solar Engineering of Thermal Processes* (4th ed.). Somerset: John Wiley & Sons, Incorporated.

Erbs, D. G., Klein, S. A., & Duffie, J. A. (1982). Estimation of the diffuse radiation fraction for hourly, daily and monthly-average global radiation. *Solar Energy*, *28*(4), 293–302. https://doi.org/10.1016/0038-092X(82)90302-4

Favoino, F., Fiorito, F., Cannavale, A., Ranzi, G., & Overend, M. (2016). Optimal control and performance of photovoltachromic switchable glazing for building integration in temperate climates. *Applied Energy*, *178*, 943–961. https://doi.org/10.1016/j.apenergy.2016.06.107

Federal Energy Management Program. (2008). *M&V Guidelines: Measurement and Verification for Federal Energy Projects (Version 3.0)*. Retrieved from https://www.hud.gov/sites/documents/DOC_10604.PDF

Goia, F., & Serra, V. (2018). Analysis of a non-calorimetric method for assessment of in-situ thermal transmittance and solar factor of glazed systems. *Solar Energy*, *166*, 458–471. https://doi.org/10.1016/j.solener.2018.03.058

Hafner, I., Rössler, M., Heinzl, B., Körner, A., Breitenecker, F., Landsiedl, M., & Kastner, W. (2012). Using BCVTB for Co-Simulation between Dymola and MATLAB for Multi-Domain Investigations of Production Plants. *Proceedings of the 9th International Modelica Conference*. Munich, Germany. https://doi.org/10.3384/ecp12076557

Hensen, J., Loonen, R., Archontiki, M., & Kanellis, M. (2015). Using building simulation for moving innovations across the 'valley of death'. *REHVA Journal*, *52*(3), 58–62.

Hunter, J. D. (2007). Matplotlib: A 2D Graphics Environment. *Computing in Science & Engineering*, *9*(3), 90–95. https://doi.org/10.1109/MCSE.2007.55

International Organization for Standardization Technical Committee 163/SC 2, C. methods. (2008). *Energy performance of buildings—Calculation of energy use for space heating and cooling* (2nd ed.: 2008-03–01). Geneva: ISO.

Jensen, S. Ø. (1995). Validation of building energy simulation programs: A methodology. *Energy and Buildings*. https://doi.org/10.1016/0378-7788(94)00910-C

Judkoff, R., & Neymark, J. (2006). Model validation and testing: The methodological foundation of ASHRAE Standard 140. *ASHRAE Transactions*.

Lawrence Berkeley National Laboratory. (2019). *BuildingsPy*. Retrieved from http://simulationresearch.lbl.gov/modelica/buildingspy/

Lomas, K. J., Eppel, H., Martin, C. J., & Bloomfield, D. P. (1997). Empirical validation of building energy simulation programs. *Energy and Buildings*, *26*(3), 253–275. https://doi.org/10.1016/S0378-7788(97)00007-8

Loonen, R., Favoino, F., Hensen, J., & Overend, M. (2017). Review of current status, requirements and opportunities for building performance simulation of adaptive facades. *Journal of Building Performance Simulation*, *10*(2), 205–223. https://doi.org/10.1080/19401493.2016.1152303

Loonen, R., Trčka, M., Cóstola, D., & Hensen, J. (2013). Climate adaptive building shells: State-of-the-art and future challenges. *Renewable and Sustainable Energy Reviews*, *25*, 483–493. https://doi.org/10.1016/j.rser.2013.04.016

Loutzenhiser, P. G., Maxwell, G. M., & Manz, H. (2007). An empirical validation of the daylighting algorithms and associated interactions in building energy simulation programs using various shading devices and windows. *Energy*. https://doi.org/10.1016/j.energy.2007.02.005

Luna-Navarro, A., Gaetani, I., Anselmo, F., Law, A., & Overend, M. (2021). The influence of occupant behaviour on the energy performance of single office space with adaptive facades: Simulation versus measured data. *Proceedings of Building Simulation Conference 2021*. Ghent, Belgium.

Luna-Navarro, A., & Overend, M. (2021). Design and validation of MATELab: A novel full-scale test room for investigating occupant perception to and interaction with façade technologies. *Building and Environment*, *203*, 108092. https://doi.org/10.1016/j.buildenv.2021.108092

Madsen, H., Bacher, P., Bauwens, G., Deconinck, A.-H., Reynders, G., Roels, S., … Lethé, G. (2016). *IEA EBC Annex 58, Report of Subtask 3, part 2: Thermal performance characterisation using time series data – statistical guidelines*. Leuven, Belgium: KU Leuven. Retrieved from https://www.iea-ebc.org/Data/publications/EBC_Annex_58_Final_Report_ST3b.pdf

Martínez, S., Erkoreka, A., Eguía, P., Granada, E., & Febrero, L. (2019). Energy characterization of a PASLINK test cell with a gravel covered roof using a novel methodology: Sensitivity analysis and Bayesian calibration. *Journal of Building Engineering*, *22*, 1–11. https://doi.org/10.1016/j.jobe.2018.11.010

Modelica Association. (2017). *Modelica*. Linköping, Sweden. Retrieved from https://www.modelica.org

MODELISAR. (2014). *FMI Standard for co-simulation*. Retrieved from https://fmi-standard.org

Moinard, S., & G.Guyon. (1999). *IEA Task 22: Empirical validation of EDF ETNA and GENEC test-cell models*.

National Renewable Energy Laboratory. (2018). *EnergyPlus*. Golden, CO, USA: DOE. Retrieved from https://github.com/NREL/EnergyPlus

Neymark, J., Judkoff, R., Knabe, G., Le, H.-T., Dürig, M., Glass, A., & Zweifel, G. (2002). Applying the building energy simulation test (BESTEST) diagnostic method to verification of space conditioning equipment models used in whole-building energy simulation programs. *Energy and Buildings*, *34*(9), 917–931. https://doi.org/10.1016/S0378-7788(02)00072-5

Nouidui, T., Lorenzetti, D. M., & Wetter, M. (2020). *EnergyPlusToFMU*. Berkeley, CA, USA: LBNL. Retrieved from http://simulationresearch.lbl.gov/fmu/EnergyPlus/export/index.html

Office of the Deputy Prime Minister. (2006). *Conservation of fuel and power: Approved Document L*.

Python Software Foundation. (2020). *Python*. Wilmington, NC, USA. Retrieved from https://www.python.org/

Roels, S. (2012). Annex 58—Reliable Building Energy Performance Characterisation Based on Full Scale Dynamic Measurements. *The International Energy Agency*.

Ruiz, G. R., & Bandera, C. F. (2017). Validation of Calibrated Energy Models: Common Errors. *Energies*, *10*(1587), 1–19. https://doi.org/10.3390/en10101587

Saelens, D., & Reynders, G. (2016). *Report of Subtask 4b: Towards a characterisation of buildings based on in situ testing and smart meter readings and potential for applications in smart grids*.

Sargent, R. G. (2013). Verification and validation of simulation models. *Journal of Simulation*, *7*(1), 12–24. https://doi.org/10.1057/jos.2012.20

Tabadkani, A., Tsangrassoulis, A., Roetzel, A., & Li, H. X. (2020). Innovative control approaches to assess energy implications of adaptive facades based on simulation using EnergyPlus. *Solar Energy*, *206*, 256–268. https://doi.org/10.1016/j.solener.2020.05.087

Taveres-Cachat, E., Favoino, F., Loonen, R., & Goia, F. (2021). Ten questions concerning co-simulation for performance prediction of advanced building envelopes. *Building and Environment*, *191*, 107570-. https://doi.org/10.1016/j.buildenv.2020.107570

Taveres-Cachat, E., & Goia, F. (2020). Co-simulation and validation of the performance of a highly flexible parametric model of an external shading system. *Building and Environment*, *182*, 107111-. https://doi.org/10.1016/j.buildenv.2020.107111

Tian, W. (2013). A review of sensitivity analysis methods in building energy analysis. *Renewable & Sustainable Energy Reviews*, *20*, 411–419. https://doi.org/10.1016/j.rser.2012.12.014

Trčka, M., Wetter, M., & Hensen, J. (2009). *An implementation of co-simulation for performance prediction of innovative integrated HVAC systems in buildings*. 724–731. Glasgow, Scotland: Lawrence Berkeley National Laboratory.

Yang, J. (2011). Convergence and uncertainty analyses in Monte-Carlo based sensitivity analysis. *Environmental Modelling & Software*, *26*(4), 444–457. https://doi.org/10.1016/j.envsoft.2010.10.007

Zhang, Y. (2012). *Use jEPlus as an efficient building design optimisation tool*. Presented at the CIBSE ASHRAE Technical Symposium, London, UK. London, UK. Retrieved from http://www.jeplus.org/wiki/lib/exe/fetch.php?media=docs:072v1.pdf

APPENDIX A BUILDING ENVELOPE CHARACTERISTICS

The test facility has internal dimensions of 5.0 m x 6.0 m x 2.5 m and is fully exposed to the outside. The required ventilation is provided by an UFAD system through a plenum below the finished floor level, and the exhaust air is extracted through the ceiling plenum. The construction and characteristics of the opaque building envelopes are shown in Table 8, and the characteristics of the transparent envelope are listed in Table 9. The internal walls are white and have a surface absorptance of approximately 0.3 and a surface emissivity of approximately 0.9.

TABLE 8 **Characteristics of opaque building envelopes of MATELab**

Component Total U-value	Layers	Thickness (m)	Density (kg/m^3)	Specific heat (J/kg^*K)
Roof	Steel sheet	0.002	8050	500
0.10 W/Km^2	Rock wool panel	0.30	22.0	1030
	Air layer	0.15	1.25	1000
	Steel PIR sandwich panel	0.040	37.0	1400
Floor	Wood floor	0.030	350	2300
0.15 W/Km^2	Cavity	0.10	1.25	1000
	Wood panel	0.030	350	2300
	Steel	0.002	8050	500
	Cavity	0.15	1.25	1000
	Steel PIR sandwich panel	0.15	37.0	1400
External wall	Wood panel	0.024	350	2300
0.175 W/Km^2	Air layer	0.020	1.25	1000
	Steel sheet	0.002	8050	500
	Steel PIR sandwich panel	0.10	37.0	1400
Internal wall	Plasterboard	0.0125	600	1090
0.50 W/Km^2	Rock wool	0.050	22.0	1030
	Plaster board	0.0125	600	1090
Glass building envelope external panel	Steel PIR sandwich panel	0.15	37.0	1400
Glass building envelope internal panel	Wood	0.050	350	2300

TABLE 9 **Characteristics of the transparent building envelopes of MATELab**

Component	Characteristics	Value
Glass building envelope	U-value	1.10 W/Km^2
	Solar heat gain coefficient	0.31
	Visible transmittance	0.50
	Solar transmittance	0.27
Internal blind	Slat width	0.035 m
	Slat separation	0.030 m
	Solar reflectance	0.65

APPENDIX B IN-SITU CHARACTERISATION OF BUILDING ENVELOPE

The in-situ characterisation included the evaluation of the most important thermal properties of the building envelope. This appendix contains detailed information on the in-situ characterisation of (i) the thermal transmittance and the solar factor of the glass façade, (ii) the air leakage flow coefficient and (iii) the thermal bridges.

B.1 THERMAL TRANSMITTANCE AND SOLAR FACTOR OF GLASS FAÇADE

To formulate the thermal performance of the building envelope as a linear and stationary steady-state thermal model, the measured data were sub-sampled by averaging it over a sufficiently long period of time. In addition, the recommendation of Madsen et al. (2016) was followed, which indicates that measurements should be averaged over periods equal to the length of the sampling time. If the test facility has a low thermal mass, a low-frequency time (equal to or less than 6 hours) is suggested. Further details of the experimental setup of the in-situ characterisation are listed in Table 10.

TABLE 10 **Measured environmental parameters with details of sensing devices and frequency of monitoring for the in-situ characterisation**

Parameter	Location	Sensor	Frequency
Heat flux	Inner building envelope surface	Hukseflux Heat flux meter	1 min
Global Solar Irradiance	Inner and outer building envelope surface	Hukseflux Pyranometer	1 min
Air temperature	Outer and inner building envelope surface	Pt100 Lastem	1 min

Following Goia & Serra (2018), the U-value U was obtained by linear regression using the ordinary least squares method and calculated as:

$$U=\left[\sum_{i}^{n}\left(\Delta T\times dq_{\mathrm{i}}\right)\right]\left[\sum_{i}^{n}\left(\Delta T_{\mathrm{i}}{}^{2}\right)\right]^{-1}$$

Equation 3

$$\Delta T=\left[T_{\mathrm{out}}-T_{\mathrm{in}}\right]$$

Equation 4

where ΔT is the temperature difference between the outdoor environment T_{out} and the indoor environment T_{in} measured in the proximity of the building envelope. dq_{i} is the heat flux measured at the glass façade at each timestep i until the final timestep n. These measurements were taken at night to minimise the effect of solar radiation on the long-wave heat transfer.

The g-value g was calculated as:

$$g = \left[\sum_{i}^{n} \left(E_{\text{out,i}} \times dq_{\text{g,i}} \right) \right] \left[\sum_{i}^{n} \left(E_{\text{out,i}}{}^{2} \right) \right]^{-1}$$

Equation 5

$$dq_{\text{g}} = \left[E_{\text{in}} + dq_{\text{E}} \right]$$

Equation 6

$$dq_{\text{E}} = \left[dq - dq_{\text{DT}} \right]$$

Equation 7

$$dq_{\Delta \text{T}} = U \times \Delta T$$

Equation 8

where $E_{\text{out,i}}$ is the solar radiation incident on the glass façade at each timestep and $dq_{\text{g,i}}$ is the solar energy transmitted through the glass, taking into account both the transmitted solar energy E_{in} and the energy transmitted by the glass due to the absorbed incident solar energy dq_{E}. To calculate dq_{E}, the heat transferred due to the difference in temperature between indoor and outdoor $dq_{\Delta \text{T}}$ must be subtracted from the total heat flow of the glass dq, which can be measured with a heat flux meter. dq can be calculated taking into account U and ΔT according to Equations 3 and 4.

B.2 AIR LEAKAGE FLOW COEFFICIENT

After performing the BDT, the data were processed according to CIBSE TM23 (CIBSE, 2000) to determine the air leakage flow coefficient C. The data obtained during the test included a series of flow rate values Q for pressure differences ΔP between indoors and outdoors:

$$Q = C(\Delta P)^{n}$$

Equation 9

where n is a coefficient that depends on the facility characteristics and can be determined from the experimental data. Transforming the above equation with natural logarithms, the following air leakage characteristic curve is obtained:

$$\ln(Q) = \ln(C) + n \times \ln(\Delta P)$$

Equation 9

The equation is obtained by linearising the data using natural logarithms and linear regression. The results must then be corrected to account for differences between actual test conditions and those of instrument calibration (CIBSE, 2000).

B.3 THERMAL BRIDGES

To quantify the effect of thermal bridges, the method proposed by Asdrubali et al. (2012) was used. This method is based on the evaluation of the incidence factor of the thermal bridges I_{tb}, which is defined as:

$$I_{tb} = \frac{U_{1D}\left(I_{tb} + I_{1D}\right) + \psi}{U_{1D}\left(I_{tb} + I_{1D}\right)}$$

Equation 9

$$U_{corrected} = I_{tb} U_{1D}\left(I_{tb} + I_{1D}\right)$$

Equation 9

where U_{1D} is the thermal transmittance without the thermal bridge, ψ is the linear thermal transmittance of the thermal bridge, l_{1D} is the length of the side of the wall perpendicular to the thermal bridge and unaffected by it, and l_{tb} is the length of the wall affected by the thermal bridge. The incidence factor of the thermal bridges, considering steady-state conditions and a constant convective coefficient, represents the ratio between the measured thermal loss, including the effect of the thermal bridge and the thermal loss of the same area of the wall without considering the effect of the thermal bridges. Therefore, the new corrected U-value $U_{corrected}$ is defined as shown in Equation 12.

The thermal images were taken for each of the locations indicated in Table 11. The images were taken at a distance of 30.0 cm from the thermal bridge to minimise possible errors due to an incorrect selection of the emissivity of the infrared camera. A FLIR T650 infrared camera was used for this assessment.

TABLE 11 **Location of the thermal bridges assessed**

Reference	Location
A	Bottom corners between south and east opaque walls and floor
B	Top corners between south and east opaque walls roof
C	Top corners between north and west opaque walls roof
D	Bottom corners between north and west opaque walls and floor
E	Junction between north and east, north and west walls
F	Junction between walls and floor
G	Junction between walls and ceiling
H	Junction between south and west, south and east walls

APPENDIX C DESCRIPTION OF MEASUREMENT CAMPAIGN

Due to ongoing research work, MATELab was only available for a limited period of time for data collection, and data were gathered between 14-21 May 2020 and 8-16 August 2020. During these periods, the parameters listed in the remainder of this appendix were collected: (i) outdoor environmental parameters, (ii) indoor environmental parameters and (iii) parameters related to the control algorithm.

C.1 OUTDOOR ENVIRONMENTAL PARAMETERS

The available weather station on MATELab's roof at the time of the experiment collected data on the dry bulb air temperature and the global solar irradiance. To evaluate the diffuse and direct components of the measured solar irradiance, a simplified approach was followed. The diffuse solar irradiance was approximated by the correlation model by Erbs, Klein, & Duffie (1982), whose accuracy was confirmed by Dervishi & Mahdavi (2012). This model calculates the ratio of the diffuse to the global solar irradiance as a function of the clearness index k_T. The average clearness index value for London, UK, in May and August was used (Duffie, 2013). Therefore, the diffuse component $I_{sol,dif}$ was evaluated as:

$$I_{sol,dif} = \left(0.9511 - 0.1604\, k_T + 4.388\, k_T^2 - 16.638\, k_T^3 + 12.336\, k_T^4\right) \times I_{sol,sky}$$

Equation 13

where $I_{sol,sky}$ is the global horizontal solar irradiance. The direct solar irradiance was then derived from the difference between the global and the diffuse solar irradiance.

When values were missing in the weather data set, the data had to be interpolated. To verify the accuracy of the measured data, dry bulb air temperature data were compared with data from a nearby weather station located on the roof of the Cambridge Computer Laboratory by the Digital Technology Group (DTG, n.d.). Nonetheless, a larger weather dataset would have been preferable to accurately determine the local boundary conditions. Ideally, direct and diffuse solar irradiance data at the weather station level should also have been measured since the control algorithm relied on the solar irradiance data and, therefore, even short-term inaccuracies could lead to incorrect or time-shifted control actions.

These data were then supplemented with humidity and wind data from an existing weather file for Cambridge created with Meteonorm v6.0 (Meteotest 2007).

C.2 INDOOR ENVIRONMENTAL PARAMETERS

Additional monitoring stations were also available to measure the indoor environmental quality at several different locations in MATELab and on the building envelope. A typical setup to monitor the influence of building envelopes on indoor environmental quality is reported in previous work (Luna-Navarro & Overend, 2021). Table 12 reports information on the sensing devices per environmental parameter and the frequency and location of the measurement.

TABLE 12 **Measured environmental parameters with details of sensing devices and frequency of monitoring for the validation**

Parameter	Location	Sensor	Frequency
Indoor dry bulb air temperature	Centre of facility	Pt100 Lastem	10 min
Surface temperature (optional)	One location	Plate Pt100 Lastem	10 min
Direct and global solar radiation	Roof of the test facility or any unobstructed location in the proximity	Weather station	1 min
Outdoor dry bulb air temperature	In the proximity of the test facility and shielded by solar radiation	Weather station	10 min
Wind speed	In the proximity of the test facility but not obstructed by the test facility or other buildings	Weather station	10 min

C.3 PARAMETERS RELATED TO THE CONTROL ALGORITHM

The movements of the blinds were monitored by a control unit, which wrote a message in a log and stored it in an internal memory when an action of the actuator was registered, i.e. when the position of a blind changed. To evaluate the accuracy of the predicted control actions during validation, the data points related to the control actions of the blind automation system were downloaded and used directly from the computer that stored the actuator messages. Other indoor and outdoor parameters triggering control actions, e.g. solar radiation incident on the building envelope and indoor and outdoor temperatures, were also used to validate blind movements.

APPENDIX D MODELLING AND SIMULATION DETAILS

This appendix provides details on the modelling and simulation of the model of MATELab. In particular, it outlines (i) the modelling parameters of the thermal model, (ii) the simulation and measurement periods and (iii) the modelling challenges of the control algorithm in the EMS feature of EnergyPlus.

D.1 MODELLING PARAMETERS OF THE THERMAL MODEL

The thermal model of MATELab was created in EnergyPlus based on the parameters reported in Section 3.3 and in Table 13.

TABLE 13 **Modelling parameters of MATELab**

Parameter	Condition
Occupancy	None
Air conditioning	None
Infiltration flow rate	0.0008 m^3/s per zone floor area
Internal heat gains	Lighting: 11.8 W/m^2
	Computer equipment: 10.0 W/m^2

D.2 SIMULATION AND MEASUREMENT PERIODS

Figure 18 shows the durations of the measurement periods (EMS: 14-21 May 2020, Dymola: 8-16 August 2020) and the simulation periods (EMS: 1-31 May 2020; Dymola: 1-31 August 2020). It highlights that the simulation periods began several days before the actual measurement periods, which was necessary to ensure that the initial conditions produced by the simulations matched those of the measured data. To determine the appropriate number of days needed to produce similar initial conditions, simulations and comparisons with the measured data were carried out in advance. In addition to the simulation period, the model was warmed up between 6 and 25 days, which was automatically determined by EnergyPlus and continued until the temperatures and heat flows in each zone converged, as described by the U.S. Department of Energy (DOE, 2018). The simulation timestep was 5 minutes.

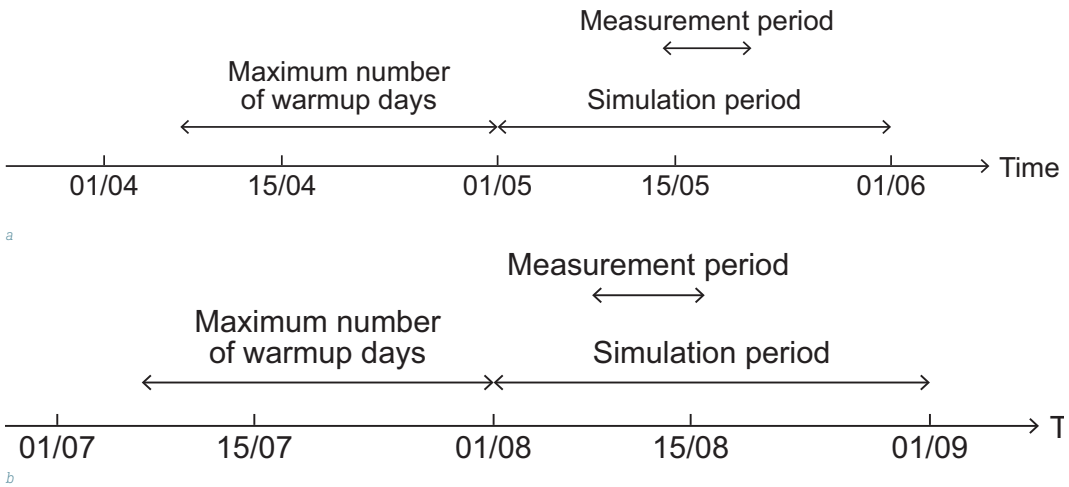

FIG. 18 Schematic of simulation and measurement periods: a. EMS feature; b. Co-simulation setup.

D.3 MODELLING CHALLENGES OF THE CONTROL ALGORITHM IN EMS FEATURE

Two aspects of the control algorithm were particularly complex to model in the EMS feature. Modelling these aspects was, however, important to reduce the modelling uncertainty and eventually obtain realistic predictions of the control actions for validation. Firstly, the monitored solar irradiance had to be used as an input to the control algorithm to ensure that the information provided to the control system was the same for the real and the predicted setup. This was achieved by using the *Schedule:File* object in EnergyPlus as a schedule, which read sub-hourly values from an external CSV file. While the input file contained 15-minute interval data, the *Interpolate to Timestep* field was set to interpolate values and use them at the appropriate minute in the hour. Secondly, the control algorithm had a time delay; since the blinds changed their position only when the solar irradiance was greater than 250 W/m^2 for more than 15 minutes. The time delay was modelled in the EMS feature through the use of trend variables, which are used to store the history of Erl variables.

APPENDIX E UNCERTAIN INPUTS USED IN MCSA

The model of MATELab had many input variables that could vary as a result of specification and modelling uncertainty. However, the variables that were likely to have an impact on the indoor air temperature – the performance indicator – were:

1. Infiltration flow rate
2. Density of building envelope cover panels
3. Specific heat capacity of building envelope cover panels
4. Ground temperature
5. Internal heat gains of equipment
6. Convective heat transfer coefficient of gap between MATELab and the ground
7. Thickness of internal partition
8. Volume of internal partition

The infiltration flow rate and the ground temperature (inputs 1 and 4) were based on measurements, and it was assumed that they follow standard normal distributions. Inputs 2 and 3 were based on the manufacturer's specifications in terms of nominal performance, which might differ from the actual performance in situ. Therefore, a standard normal distribution was assumed, and the minimum and maximum values found in the literature were used (CIBSE, 2015). The input variables 5 to 6 reflect variations in building specifications, for which only minima and maxima were known. They were also regarded as standard normal distributions where extreme values were less likely to be selected than values near the mean. Since the tails of a standard normal distribution extend indefinitely, the previously described LHS method may generate negative numbers that are usually not supported by EnergyPlus. They represented only a very small proportion of the total number of samples and were thus set to zero.

The last two input variables (7 and 8) were design parameters, which were defined by the authors and could be changed through interventions. Therefore, they were assumed to be uniformly distributed as they may be regarded as being equally probable. The sources used to inform the shape of the distributions can be seen in Table 14.

TABLE 14 **Input variables used in MCSA, including their symbol, assumed distribution, type of variation and source**

Input variable	Symbol (unit)	Distribution assumed	Uncertainty type	Source
Infiltration flow rate	Q_{inf} ($m^3/s\ m^2$)	N (0.003,0.0008)	Modelling uncertainty	Measured
Density	p (kg/m^3)	N (1500,333)	Specification uncertainty	Technical sheet from manufacturer
Specific heat capacity	c (J/kgK)	N (5000,1000)	Specification uncertainty	Technical sheet from manufacturer
Ground temperature	T_g (°C)	N (20.0,1.7)	Modelling uncertainty	Measured
Internal heat gains	Q_{int} (W/m^2)	U (100,33.3)	Modelling uncertainty	CIBSE (2015, Table 1)
Convective heat transfer coefficient of gap	h_c (W/m^2K)	U (1.5,0.5)	Modelling uncertainty	CIBSE (2015, Table 3.7)
Thickness	d (m)	U (0.2,0.07)	Specification uncertainty	Defined by authors
Volume	V (m^3)	U (20.0,6.7)	Specification uncertainty	Defined by authors

APPENDIX F RESULTS OF IN-SITU MEASUREMENTS

This appendix begins by presenting the results of the in-situ measurements of the U-values and then goes on to describe the analysis of the thermal bridges using infrared images.

TABLE 15 **Results of the in-situ measurements of the U-values**

ID	Zone	Area (m^2)	U-value (W/Km^2)	Total U-value (W/Km^2)
A	Left side	0.438	1.225	1.232
B	Top side	0.373	1.152	
C	Bottom side	0.373	1.069	
D	Centre side	0.578	0.969	
E	Top edge	0.246	1.410	
F	Bottom edge	0.246	1.210	
G	Left edge	0.321	1.559	
H	Right side	0.438	1.225	
I	Right edge	0.321	1.559	

Figure 19 shows the thermal bridge type F (Table 15) with the thermal image (Figure 18a) and the corresponding calculated temperature profile along a 0.77 m long line on the wall (Figure 18b). The results of the full thermal bridge assessment using infrared images are reported in Table 16. The average indoor air temperature was 22.6 °C, while the temperature in the homogeneous wall areas was around 22.1°C. The corresponding value of the incidence factor of the thermal bridge calculated from Equation 11 was 1.17, as reported in Table 16. To evaluate the total thermal losses taking into account the thermal bridge effect, the corrected U-value $U_{corrected}$ was calculated according to Equation 12, where I_{tb} was the weighted average of the several I_{tb} affecting each surface.

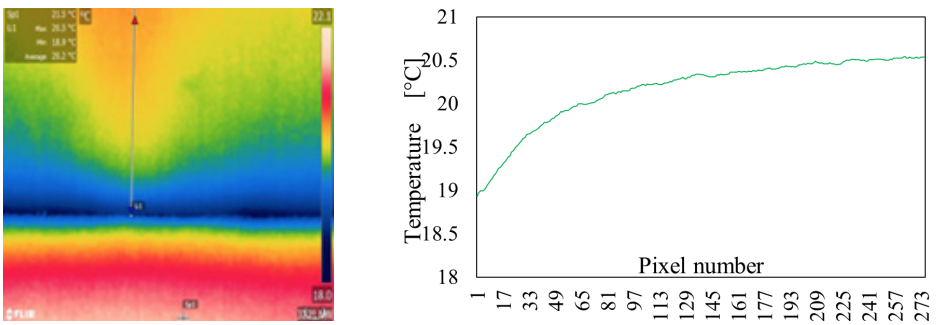

a b

FIG. 19 Thermal bridge assessment for type F: a. Thermal image; b. Temperature profile across the wall.

TABLE 16 **Quantitative analysis of infrared images**

ID	Typology and description of thermal bridge	I_{tb}	Affected surfaces
A	Bottom corners on south building envelope (floor-wall-wall)	1.26	Floor and east, south and west walls
B	Top corners on south building envelope (roof-wall-wall)	1.12	Roof and east, south and west walls
C	Top corners on north building envelope (roof-wall-wall)	1.09	Roof and east, north and west walls
D	Bottom corners on north building envelope (floor-wall-wall)	1.18	Floor and east, north and west walls
E	Vertical corner lines wall-wall (wall-wall)	1.14	All walls
F	Horizontal corner lines wall-floor	1.17	Floor and wall
G	Horizontal corner lines wall-roof (roof-wall)	1.11	East and west walls
H	Vertical lines wall-wall interface (junction of 2 wall parts on south building envelope)	1.13	South wall